Thermodynamic modeling of supercooled water

V. Holten, C. E. Bertrand,* M. A. Anisimov, and J. V. Sengers
Institute for Physical Science and Technology and
Department of Chemical and Biomolecular Engineering,
University of Maryland, College Park, Maryland 20742, U.S.A.

Technical Report
prepared for the
International Association for the Properties of Water and Steam
(September 2011)

---

*Current address: Department of Nuclear Science and Engineering, Massachusetts Institute of Technology, Cambridge, MA 02139

Table of Contents

Abstract

A status report is presented concerning the currently available experimental information for the thermodynamic properties of supercooled water and the possibility of modeling these thermodynamic properties on a theoretical basis. Part of the interest into the thermodynamic behavior of supercooled water is caused by an anomalous temperature dependence of the heat capacity, the compressibility and the thermal expansivity. Extrapolation of the IAPWS-95 Formulation for the Thermodynamic Properties of H_2O cannot account for the available thermodynamic information satisfactorily. We show that by assuming the existence of a liquid–liquid critical point, the theory of critical phenomena can give an accurate account of the experimental thermodynamic-property data up to a pressure of 150 MPa. In addition, we show that a phenomenological extension of the theoretical model can account for the experimental data to 400 MPa. Remaining theoretical issues that still need to be resolved are elucidated. Nevertheless, the information provided in this report shows that the critical-point parametric equation of state describes the available thermodynamic data on supercritical water within experimental accuracy, thus establishing a benchmark for any further developments in this area.

1 Introduction

The peculiar thermodynamic behavior of supercooled water is currently receiving considerable attention. Upon supercooling, water exhibits an anomalous increase of its isobaric heat capacity and its isothermal compressibility, and an anomalous decrease of its expansivity coefficient [1]. One thermodynamically consistent explanation, originally proposed by Poole et al. [2], is based on the presumed existence of a liquid–liquid critical point (LLCP) in water deep in the supercooled region. The hypothesis of the existence of a critical point in metastable water has been considered by many authors as recently reviewed by Bertrand and Anisimov [3]. In addition, several authors have made attempts to develop a thermodynamic model for the thermodynamic properties of supercooled water based on the LLCP scenario [3–7]. The existence of a liquid–liquid critical point in supercooled water is still being debated [8,9]. The purpose of this technical report is to demonstrate that a theoretical model based on the presumed existence of a second critical point in water is capable of representing the available experimental thermodynamic property data for supercooled water.

This report is organized as follows. In Section 2 we provide an assessment of the IAPWS-95 formulation [10,11] for the thermodynamic properties of H_2O for water at temperatures above the melting temperature when extrapolated into the supercooled region, confirming the need for an improved equation of state for supercooled water. In Section 3 we review the currently available experimental information for the thermodynamic properties of supercooled water. In Section 4 we formulate a thermodynamic model for supercooled water by adopting suitable physical scaling fields relative to the location of a liquid–liquid critical point in metastable water. In Section 5 we show that this theoretical model does yield an accurate representation of the thermodynamic property data of supercooled water up to pressures of 150 MPa. In Section 6 we present a phenomenological extension of the theoretical model and show that this extension allows a representation of all experimental data for supercooled water up to the maximum available pressure of 400 MPa. The report concludes with a discussion of the results and of some related issues in Section 7.

2 IAPWS-95 formulation in the supercooled region

The performance of IAPWS-95 in the supercooled metastable region has been assessed first by Wagner and Pruß [11] and, more recently, by an IAPWS task group on “IAPWS-95 properties in the metastable region of seawater freezing point lowering” in 2007 [12]. The task group performed a literature search in 2005 and did not find any new data in the supercooled region that had not been mentioned in the earlier paper of Wagner and Pruß [11]. Hence, the task group concluded that the IAPWS-95 formulation agreed with existing experimental data of supercooled water at ordinary pressures. The task group also concluded that there were no data for

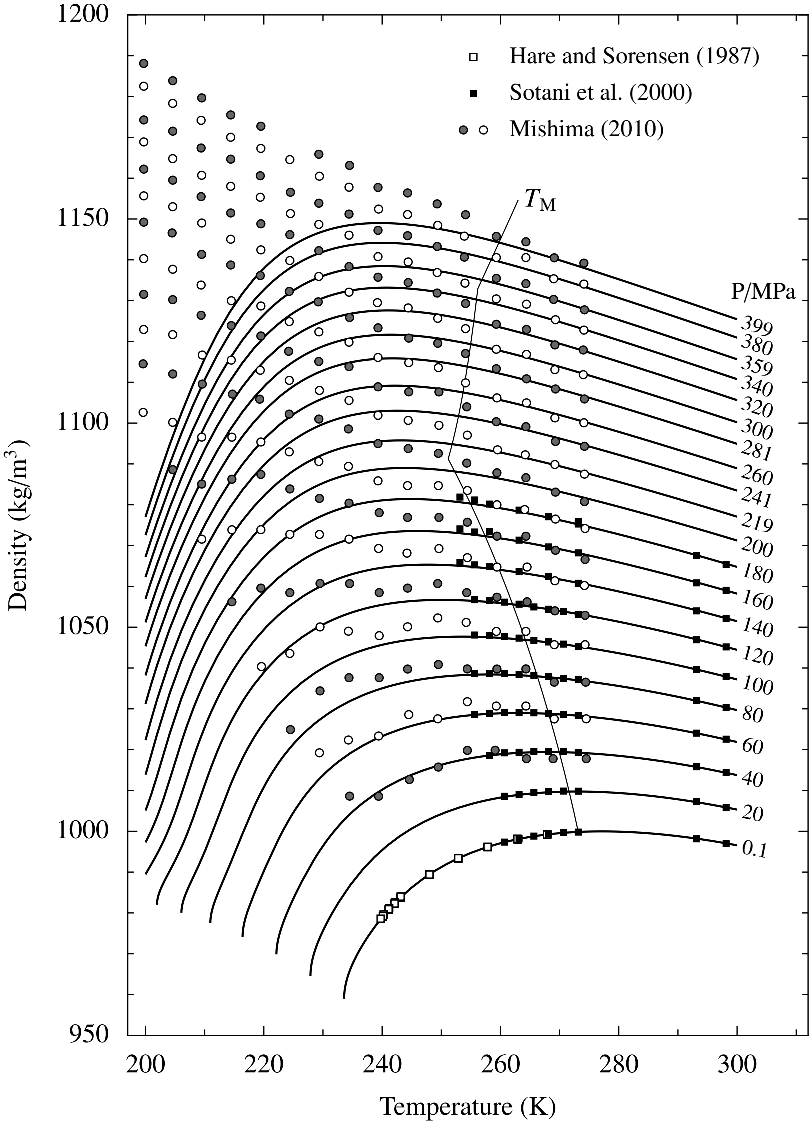

Figure 1: Densities according to IAPWS-95 (curves). IAPWS-95 is valid to the right of the melting curve T_M; the IAPWS-95 values left of the melting curve are extrapolations. The symbols represent experimental data of Mishima [13], Sotani et al. [14] and Hare and Sorensen [15]. The symbols for Mishima's densities on different isobars are alternatingly open and filled to guide the eye. Mishima's data have been corrected as described in Sec. 3.1.

supercooled water at high pressures.

However, there are compressibility data of Kanno and Angell (1979) up to 190 MPa [18], expansivity data of Ter Minassian et al. (1981) up to 400 MPa [16], density data of Sotani et al. (2000) up to 200 MPa [14], of Asada et al. (2002) up to 380 MPa [19] and of Mishima (2010) up to 400 MPa [13]. A comparison of the densities calculated from the IAPWS-95 formulation with the experimental density data of Hare and Sorensen (1987) [15], of Sotani et al. (2000) [14], and of Mishima (2010) [13] is shown in Fig. 1. While the IAPWS-95 formulation does indeed represent the experimental density data at ambient pressure, the deviations from the formulation become larger and larger with increasing pressure. Especially at higher pressures, there is a sizable discrepancy between the IAPWS-95 formulation and the experimental data; the slope (or the expansivity) has even a different sign. According to Wagner and Pruß [11], the behavior of the expansivity coefficient α_V calculated from the IAPWS-95 formulation should be reasonable in the liquid region at low temperature. However, from Fig. 2 we see that the IAPWS-95 expansivity is in error by up to 50% in the low-temperature region even at temperatures above the melting temperature where the IAPWS-95 formulation should be

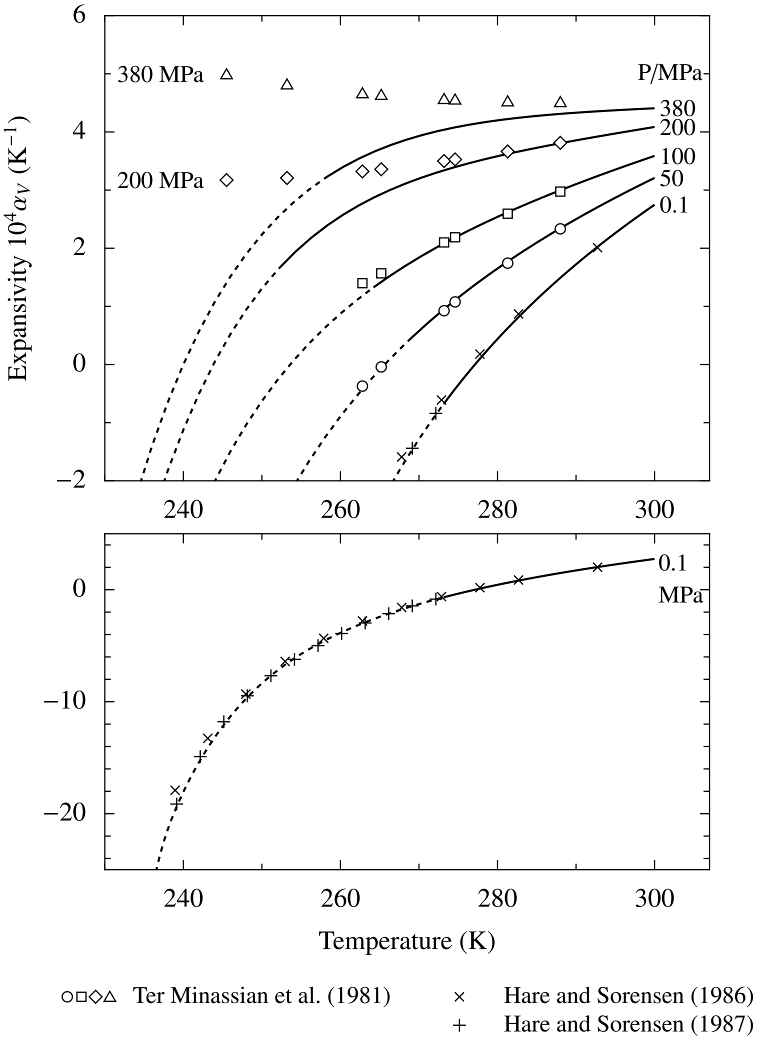

Figure 2: Expansivity coefficient according to IAPWS-95 (solid curves: within region of validity, dashed curves: extrapolation). Symbols represent experimental data of Ter Minassian et al. [16] and Hare and Sorensen [15,17].

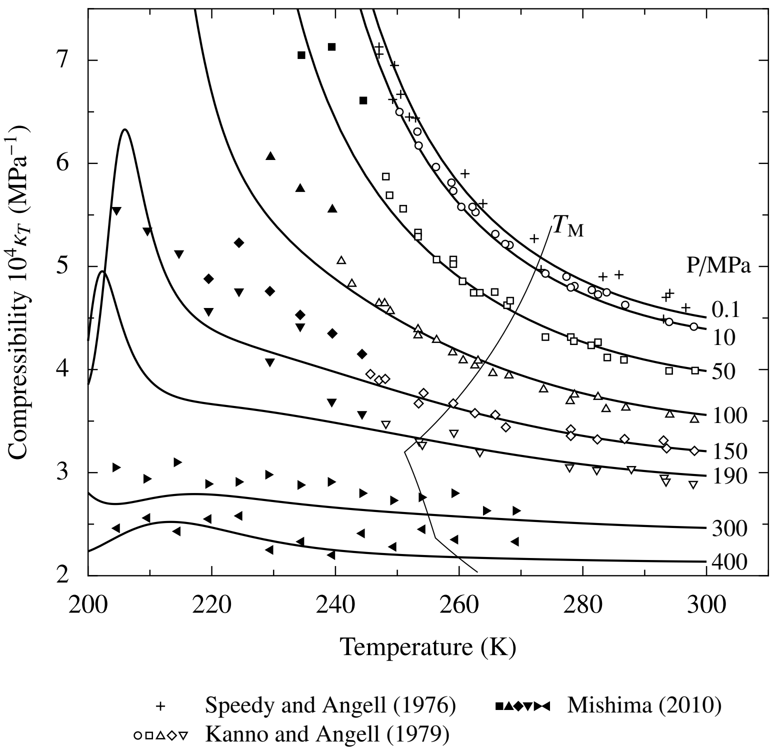

Figure 3: Isothermal compressibility according to IAPWS-95 (curves). IAPWS-95 is valid to the right of the melting curve T_M; the IAPWS-95 values left of the melting curve are extrapolations. Symbols represent experimental data of Speedy and Angell [20], Kanno and Angell [18], and Mishima [13]. Solid and open symbols with the same shape correspond to the same pressure.

valid. The isothermal compressibility κ_T calculated from the IAPWS-95 formulation agrees with the experimental data down to about 250 K and up to 400 MPa, as shown in Fig. 3. However, at lower temperatures, the IAPWS-95 compressibilities do not even qualitatively agree with the data.

In the supercooled region, IAPWS-95 predicts a re-entrant liquid spinodal, as shown in Fig. 4. The spinodal pressure becomes positive at 233.6 K, which is a few degrees below the homogeneous nucleation limit. At about 195 K and 175 MPa, the spinodal curve crosses the homogeneous nucleation limit and enters the region where supercooled water can be experimentally observed. Up to about 290 MPa, the spinodal curve stays in the experimentally accessible range. Since a spinodal has not been observed there, the spinodal of IAPWS-95 contradicts experimental evidence. More fundamentally, a re-entrant spinodal is problematic because it has been shown to be thermodynamically implausible [1,23].

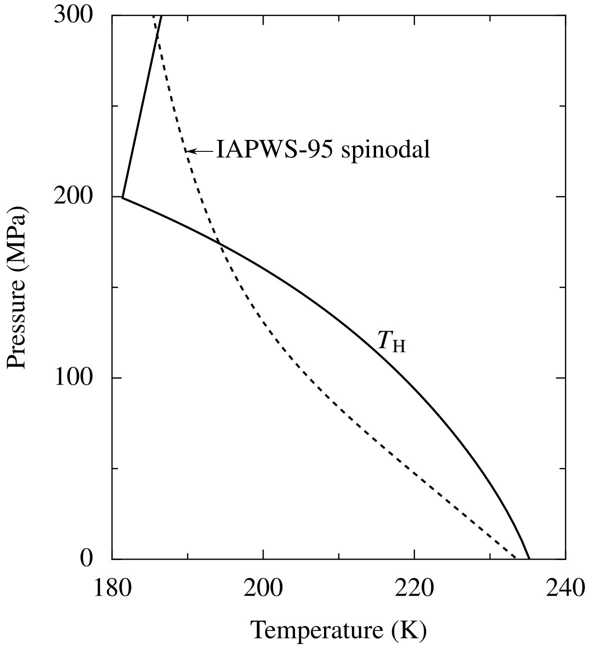

Figure 4: Location of the liquid spinodal according to the IAPWS-95 formulation. The curved marked with T_H is the homogeneous ice nucleation limit [21,22].

3 Review of experimental data

3.1 Density data

Since the IAPWS-95 formulation was developed, new data for the density for supercooled water have been reported. Most notable is the recent work of Mishima [13], who measured the density and compressibility down to 200 K and up to 400 MPa (Fig. 5). More accurate density measurements have been published by Sotani et al. [14] and Asada et al. [19], but their lowest temperature is 253 K, so in a larger temperature range Mishima's data are the only data available.

The density data of Mishima show systematic differences of up to 5 kg/m^3 with the densities reported by Asada et al., with IAPWS-95 (in the region where it is reliable), and with the equation of state of Saul and Wagner [25]. The differences appear to be mostly pressure dependent and only slightly temperature dependent; see Fig. 6. In the range from 273 K to 373 K and 0 MPa to 380 MPa, where the three other data sets (Asada et al., IAPWS-95, Saul and Wagner) overlap and can

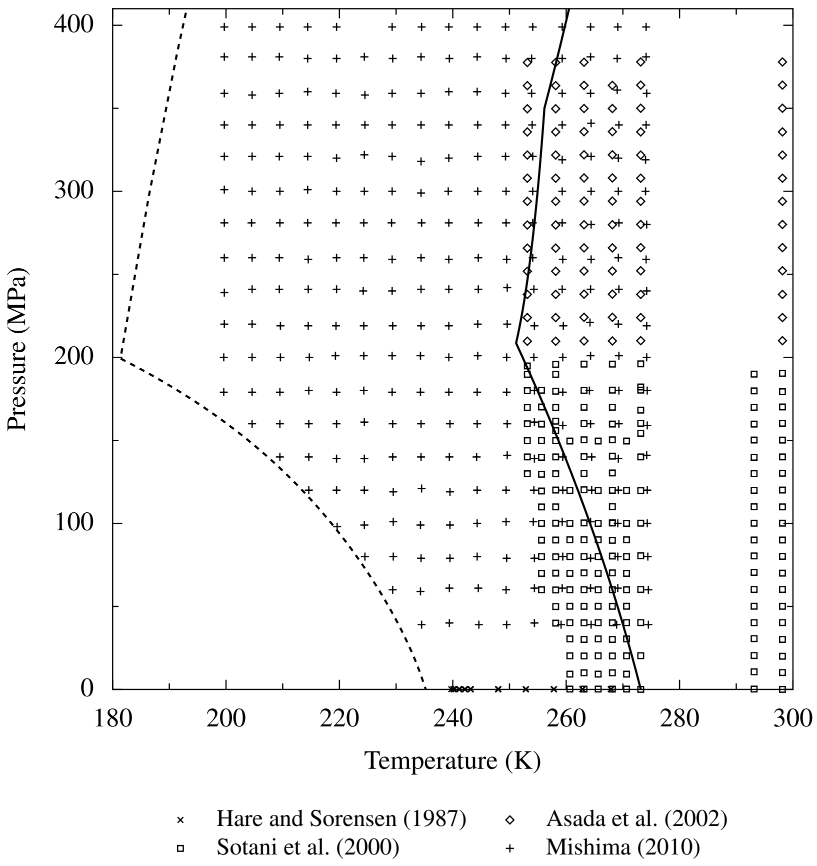

Figure 5: Location of the experimental density data [13–15,19]. The solid curve is the ice–liquid phase boundary [24]; the dashed curve is the homogeneous ice nucleation limit [21,22]. The location of the dashed curve above 300 MPa is uncertain.

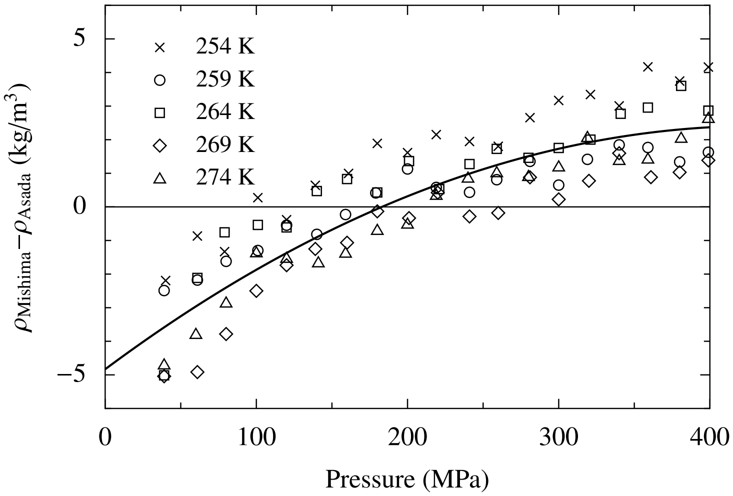

Figure 6: Difference of Mishima's [13] density and the correlation of Asada et al. [19]. The curve is a quadratic fit, $\Delta\rho = -4.83 + 0.03348P - 3.87 \times 10^{-5}P^2$, with $\Delta\rho$ in kg/m^3 and pressure P in MPa.

be considered reliable, their maximum mutual difference is 0.8 kg/m^3. Therefore, we decided that a correction of the Mishima data is justified. A pressure-dependent density correction was determined by fitting a quadratic function of the pressure to the difference of Mishima's densities and the correlation* of Asada et al., between 245 K and 274 K (Fig. 6). This density correction was then subtracted from all densities measured by Mishima.

The accurate densities measured by Sotani et al. [14] and Asada et al. [19] are not tabulated but only given in graphs. Furthermore, these graphs do not show the densities themselves but only their deviation from a reference correlation (the Saul–Wagner 1989 equation of state in the paper of Sotani et al. and IAPWS-95 in the article of Asada et al.). Multiple attempts to obtain the original data from the authors of the two articles have failed, so the data were extracted from the graphs. The conversion causes an uncertainty in the pressure of about 0.5 MPa.

At atmospheric pressure, Hare and Sorensen [15] measured the density down to 240 K. They showed that their measurements were not affected by the 'excess density' effect, which occurs in thin capillary tubes and caused too large densities in some experiments of others.

The only experimental water density data to which the IAPWS-95 formulation was fitted in the supercooled liquid region are those from Kell [26]. According to Wagner and Pruß [11], these data are "very accurate". However, the density values [27] came from a fit that is valid only above the freezing point but was extrapolated down to −37 °C, while Kell cautioned that no claim for the accuracy of extrapolated values could be made. Coincidentally, the extrapolated fit of Kell agrees with Hare

---

* There is a sign error in the correlation of Asada et al. [19]: the coefficient a_6 in their Table 1 should have a positive sign.

and Sorensen's [15] data. Therefore, if the IAPWS-95 formulation had been fitted to Hare and Sorensen's data instead of Kell's fit, the result would probably have been almost the same.

3.2 Density-derivative data

Both the isothermal compressibility and the expansivity coefficient of supercooled water have been measured (Fig. 7). The most accurate compressibility data are from Kanno and Angell [18], whereas Mishima's [13] data cover the largest temperature range. The only expansivity measurements are from Ter Minassian et al. [16]. Hare and Sorensen [15,17] also published expansivities (at 0.1 MPa), but these were obtained from the derivative of a fit to their density data.

The data from Speedy and Angell [20] and Kanno and Angell [18] were digitized from their graphs. Ter Minassian et al. [16] provide an empirical correlation that reproduces their data.

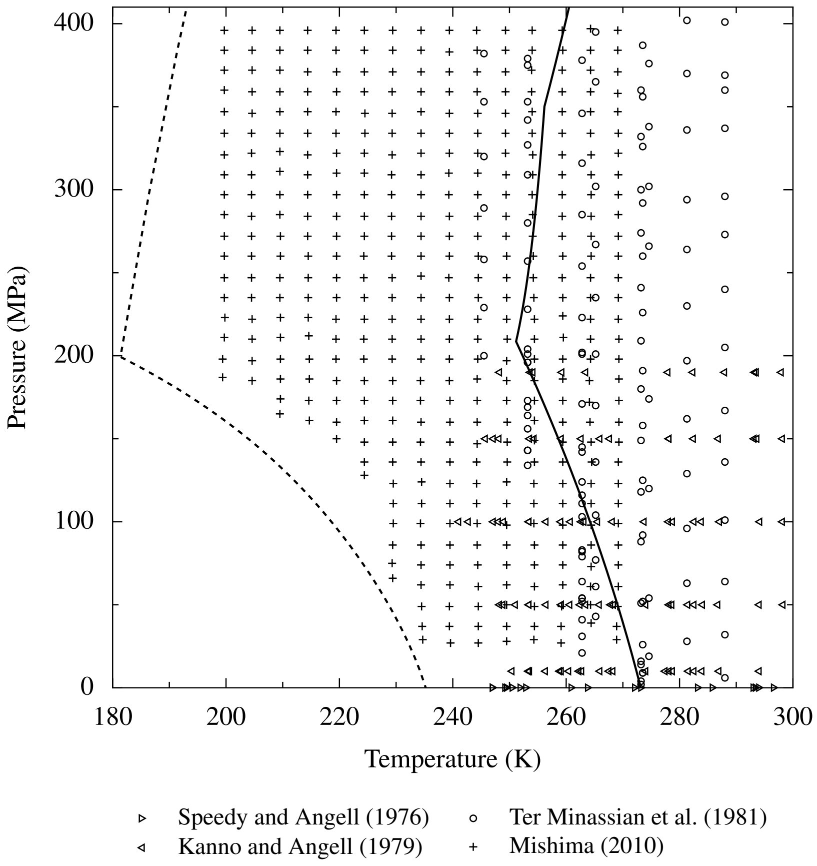

Figure 7: Location of the experimental density-derivative data. Ter Minassian et al. [16] measured the expansivity coefficient, the other authors [13,18,20] measured the isothermal compressibility.

3.3 Heat-capacity data

The isobaric heat capacity of supercooled water has been measured only at atmospheric pressure. Measurements by Anisimov et al. [28] down to 266 K already showed anomalous behavior. Angell et al. [29,30] extended the range of measurements down to 236 K. Recent measurements by Archer and Carter [31], also down to 236 K, do not agree with those of Angell et al. [30]. Archer and Carter suggest that the temperature calibration procedure of Angell et al. caused a systematic error in their measurements. Furthermore, Archer and Carter suspect that measurements of Tombari et al. [32] (down to 245 K) were also affected by systematic calorimetric errors.

In the stable region, there exist heat-capacity measurements up to 100 MPa by Sirota et al. [33] with an uncertainty of 0.3%. Although Wagner and Pruß [11] claim that IAPWS-95 represents all data to within the experimental uncertainty, IAPWS-95 systematically deviates from part of the data of Sirota et al.. For the data at 273 K, the mean deviation is 0.4%, with individual points deviating up to 0.6%. However, at 273 K IAPWS-95 agrees with the expansivity correlation of Ter Minassian et al., with which a comparison can be made by using a thermodynamic relation for the isothermal pressure derivative $(\partial C_P/\partial P)_T$ of the isobaric heat capacity C_P. Therefore, the data of Sirota et al. have not been used in our analysis.

Recently, Manyà et al. [34] have measured the heat capacity at 4 MPa from 298 K to 465 K. Although this range does not include supercooled states, their lowest-temperature results could be used in principle to improve the behavior of our model. However, it turns out that the results of Manyà et al. imply that $(\partial C_P/\partial P)_T > 0$ for pressures lower than 4 MPa, which contradicts the thermodynamic relation $(\partial C_P/\partial P)_T = -T(\partial^2 V/\partial T^2)_P$, with V being the molar volume. Hence, the data of Manyà et al. will not be considered.

3.4 Liquid–liquid coexistence curve

Both the existence of a second critical point and its location are still being debated in the literature. If the second critical point exists, there should be a liquid–liquid transition (LLT) curve – separating a hypothetical high-density liquid and low-density liquid – which ends at the critical point. At pressures below the critical pressure, water's response functions exhibit an extremum near the Widom line, which is the extension of the LLT curve into the one-phase region and the locus of maximum fluctuations.

While the location of the critical point obtained by different simulations varies greatly, different attempts to locate the LLT and the Widom line from experimental data have yielded approximately the same result. Kanno and Angell [18] fitted power laws to their compressibility measurements and obtained singular temperatures located 5 K to 12 K below the homogeneous nucleation temperature T_{H} (Fig. 8), suggesting a LLT that mimics the T_{H} curve but shifted to lower temper-

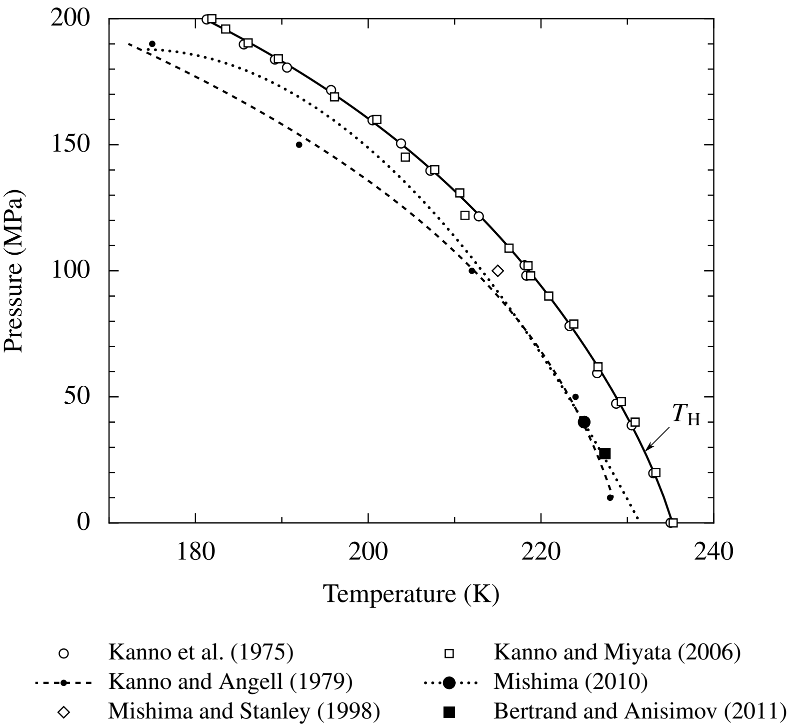

Figure 8: Homogeneous nucleation temperatures (open circles [21] and squares [22] and fitted solid curve), Mishima's [13] conjectured liquid–liquid coexistence curve (dotted) and critical point (cross), and Kanno and Angell's curve (dashed) connecting the fitted singular temperatures (solid circles) [18]. Open diamond: bend in the melting curve of ice IV [35]; plus sign: critical point of Bertrand and Anisimov [3].

ature. Mishima measured metastable melting curves of H_2O ice IV [35] and D_2O ices IV and V [36], and found that they suddenly bent at temperatures of 4 K to 7 K below T_H. According to Mishima, this is indirect evidence for the location of the LLT, but a one-to-one correspondence between a break in the melting curve and the LLT has been questioned by Imre and Rzoska [37].

Mishima [13] approximated the LLT by a quadratic function of T with approximately the same shape as the T_H curve, but allowing a shift to lower temperature. His final result, shown in Fig. 8, is close to Kanno and Angell's curve for pressures up to 100 MPa, albeit with a different curvature.

4 Thermodynamic model for supercooled water

4.1 Scaling fields and thermodynamic properties

Fluids belong to the universality class of Ising-like systems whose critical behavior is characterized by two independent scaling fields, a "strong" scaling field h_1 (ordering field) and a "weak" scaling field h_2, and by a dependent scaling field h_3 which asymptotically close to the critical point becomes a generalized homogeneous function of h_1 and h_2 [38–40]:

$$h_3(h_1,h_2) \approx |h_2|^{2-\alpha} f^{\pm}\left(\frac{h_1}{|h_2|^{2-\alpha-\beta}}\right). \tag{1}$$

In this expression $\alpha \simeq 0.110$ and $\beta \simeq 0.3265$ are universal critical exponents [41, 42] and $f^{\pm}$, with the superscripts $\pm$ referring to $h_2 > 0$ and $h_2 < 0$, is a universal scaling function except for two system-dependent amplitudes. Associated with these scaling fields are two conjugate scaling densities, a strongly fluctuating scaling density ϕ_1 (order parameter) and a weakly fluctuating scaling density ϕ_2, such that

$$\mathrm{d}h_3 = \phi_1\,\mathrm{d}h_1 + \phi_2\,\mathrm{d}h_2 \tag{2}$$

with

$$\phi_1 = \left(\frac{\partial h_3}{\partial h_1}\right)_{h_2}, \qquad \phi_2 = \left(\frac{\partial h_3}{\partial h_2}\right)_{h_1}. \tag{3}$$

In addition one can define three susceptibilities, a "strong" susceptibility χ_1, a "weak" susceptibility χ_2, and a "cross" susceptibility χ_{12}:

$$\chi_1 = \left(\frac{\partial \phi_1}{\partial h_1}\right)_{h_2}, \quad \chi_2 = \left(\frac{\partial \phi_2}{\partial h_2}\right)_{h_1}, \quad \chi_{12} = \left(\frac{\partial \phi_1}{\partial h_2}\right)_{h_1} = \left(\frac{\partial \phi_2}{\partial h_1}\right)_{h_2}. \tag{4}$$

In fluids and fluid mixtures one encounters a large variety of different types of critical phenomena [43]. The asymptotic thermodynamic behavior near all kinds of critical points can be described in terms of Eq. (1). The differences arise from the actual relationships between the scaling fields and the physical fields [44], subject to the condition that at the critical point

$$h_1 = h_2 = h_3 = 0. \tag{5}$$

In one-component fluids the relevant physical fields are the chemical potential μ (Gibbs energy per mole), the temperature T, and the pressure P. To satisfy condition (5) one defines $\Delta\mu = \mu - \mu_\mathrm{c}$, $\Delta T = T - T_\mathrm{c}$, and $\Delta P = P - P_\mathrm{c}$. In this report we adopt the usual convention that a subscript c refers to the value of the property at the critical point. There are two special models for critical behavior that deserve some attention. The first is the lattice gas in which the ordering field h_1 is asymptotically proportional to $\Delta\mu$ and the weak scaling field proportional to ΔT [45–47]. Hence, in the lattice gas ϕ_1 is proportional to $\Delta\rho = \rho - \rho_c$ and ϕ_2 proportional to $\Delta s = s - s_c$, where ρ is the mass density and s the entropy density. The lattice gas provides a model for the vapor–liquid critical point where the mass density yields the major contribution to the order parameter. In practice, the asymptotic critical behavior of a fluid near the critical point, including that of H_2O [48], can be described by a slight modification of the lattice-gas model to account for some lack of vapor–liquid symmetry in real fluids. Another special model is a lattice liquid in which the ordering field is asymptotically proportional to ΔT and in which the weak scaling field is proportional to $\Delta\mu$ [3]. Near the liquid–liquid critical point in supercooled water the entropy yields the major contribution to the order parameter and not the mass density, as first pointed out by Fuentevilla and Anisimov [6]. Thus the thermodynamic properties near this liquid–liquid critical point can be described by a slight modification of the lattice-liquid model to account for some lack of symmetry in the order parameter [3].

To implement a scaled thermodynamic representation it is convenient to make all thermodynamic properties dimensionless in terms of the critical parameters T_c and ρ_c or $V_c = \rho_c^{-1}$:

$$\hat{T} = \frac{T}{T_c}, \quad \hat{\mu} = \frac{\mu}{RT_c}, \quad \hat{P} = \frac{PV_c}{RT_c}, \tag{6}$$

where R is the ideal-gas constant. For the dimensionless physical densities we define

$$\hat{V} = \frac{V}{V_c}, \quad \hat{S} = \frac{S}{R}, \quad \hat{C}_P = \frac{C_P}{R}, \tag{7}$$

where V is the molar volume, S the molar entropy, and C_P the isobaric molar heat capacity. The thermodynamic model of Bertrand and Anisimov was formulated in terms of $\hat{P}(\hat{\mu}, \hat{T})$ for which

$$\mathrm{d}\hat{P} = \hat{V}^{-1}\mathrm{d}\hat{\mu} + \hat{V}^{-1}\hat{S}\,\mathrm{d}\hat{T}. \tag{8}$$

We have found it more convenient to formulate the thermodynamic model in terms of $\hat{\mu}(\hat{P}, \hat{T})$ for which

$$\mathrm{d}\hat{\mu} = \hat{V}\,\mathrm{d}\hat{P} - \hat{S}\,\mathrm{d}\hat{T}. \tag{9}$$

Thus in our model we identify the order parameter with the entropy itself instead of the entropy density. In our model the scaling fields are related to the physical fields as

$$h_1 = \Delta\hat{T} + a'\Delta\hat{P}, \tag{10}$$

$$h_2 = -\Delta\hat{P} + b'\Delta\hat{T}, \tag{11}$$

$$h_3 = \Delta\hat{P} - \Delta\hat{\mu} + \Delta\hat{\mu}^{\mathrm{r}}, \tag{12}$$

with

$$\Delta\hat{T} = \frac{T - T_c}{T_c}, \quad \Delta\hat{P} = \frac{(P - P_c)V_c}{RT_c}, \quad \Delta\hat{\mu} = \frac{\mu - \mu_c}{RT_c}. \tag{13}$$

In Eq. (10) a' represents the limiting slope $-\mathrm{d}\hat{T}/\mathrm{d}\hat{P}$ of the phase-coexistence or Widom line. In Eq. (11) b' is a so-called mixing coefficient which accounts for the fact that the critical phase transition in supercooled water is not completely symmetric in terms of the entropy order parameter. Introduction of mixing of this type is also known in the literature as revised-scaling approximation [49]. Equation (1) only represents the asymptotic behavior of the so-called singular critical contributions to the thermodynamic properties. To obtain a complete representation of the thermodynamic properties we need to add a regular (i.e., analytic) background contribution. As has been common practice in developing scaled equations of state in fluids near the vapor-liquid critical point [48,49], the regular background contribution is represented by a truncated Taylor-series expansion around the critical point:

$$\Delta\hat{\mu}^{\mathrm{r}} = \sum_{m,n} c_{mn}(\Delta\hat{T})^m(\Delta\hat{P})^n, \quad \text{with} \quad c_{00} = c_{10} = c_{01} = 0. \tag{14}$$

The first two terms in the temperature expansion of $\Delta\hat{\mu}^{\mathrm{r}}$ depend on the choice of zero entropy and energy and do not appear in the expressions of any of the physically observable thermodynamic properties. Hence, these coefficients may be set to zero. Furthermore, the coefficient $c_{01} = \hat{V}_{\mathrm{c}} - 1 = 0$. Strictly speaking, critical fluctuations also yield an analytic contribution to h_3 [50,51]. In this report we incorporate this contribution into the linear background contribution as has also been done often in the past.

From the fundamental thermodynamic differential relation (9) it follows that

$$\hat{V} = \left(\frac{\partial\hat{\mu}}{\partial\hat{P}}\right)_{\hat{T}} = 1 - a'\phi_1 + \phi_2 + \Delta\hat{\mu}^{\mathrm{r}}_{\hat{P}}, \tag{15}$$

$$\hat{S} = -\left(\frac{\partial\hat{\mu}}{\partial\hat{T}}\right)_{\hat{P}} = \phi_1 + b'\phi_2 - \Delta\hat{\mu}^{\mathrm{r}}_{\hat{T}}. \tag{16}$$

In this report we adopt the convention that a subscript $\hat{P}$ indicates a derivative with respect to $\hat{P}$ at constant $\hat{T}$ and a subscript $\hat{T}$ a derivative with respect to $\hat{T}$ at constant $\hat{P}$. Finally, the dimensionless isothermal compressibility $\hat{\kappa}_T$, expansivity coefficient $\hat{\alpha}_V$, and isobaric heat capacity $\hat{C}_P$ can be expressed in terms of the scaling susceptibilities χ_1, χ_2, and χ_{12}:

$$\hat{\kappa}_T = -\frac{1}{\hat{V}}\left(\frac{\partial\hat{V}}{\partial\hat{P}}\right)_T = \frac{1}{\hat{V}}\left[(a')^2\chi_1 + \chi_2 - 2a'\chi_{12} - \Delta\hat{\mu}^{\mathrm{r}}_{\hat{P}\hat{P}}\right], \tag{17}$$

$$\hat{\alpha}_V = \frac{1}{\hat{V}}\left(\frac{\partial\hat{V}}{\partial\hat{T}}\right)_P = \frac{1}{\hat{V}}\left[-a'\chi_1 + b'\chi_2 + (1 - a'b')\chi_{12} + \Delta\hat{\mu}^{\mathrm{r}}_{\hat{T}\hat{P}}\right], \tag{18}$$

$$\hat{C}_P = \hat{T}\left(\frac{\partial\hat{S}}{\partial\hat{T}}\right)_P = \hat{T}\left[\chi_1 + (b')^2\chi_2 + 2b'\chi_{12} - \Delta\hat{\mu}^{\mathrm{r}}_{\hat{T}\hat{T}}\right]. \tag{19}$$

4.2 Parametric equation of state

It is not possible to write the scaled expression (1) for h_3 as an explicit function of h_1 and h_2. Such attempts always cause singular behavior of the thermodynamic potential in the one-phase region either at $h_1 = 0$ or at $h_2 = 0$. This problem is solved by replacing the two independent scaling fields, h_1 and h_2, with two parametric variables: a variable r which measures a "distance" from the critical point and an angular variable θ which measures the location on a contour of constant r. A transformation most frequently adopted has the form:

$$h_1 = a r^{2-\alpha-\beta}\theta(1-\theta^2), \qquad h_2 = r(1-b^2\theta^2). \tag{20}$$

From Eqs. (1) and (3) it then follows that the order parameter ϕ_1 must have the form [52]:

$$\phi_1 = k r^{\beta} M(\theta), \tag{21}$$

where $M(\theta)$ is a universal analytic function of θ. In principle, this function can be calculated from the renormalization-group theory of critical phenomena [53]. In practice one adopts an analytic approximant for $M(\theta)$, the simplest one being $M(\theta) = \theta$ [54]:

$$\phi_1 = k r^{\beta}\theta. \tag{22}$$

Equations (20) and (22) define what is known as the "linear model" parametric equation of state. In these equations a and k are two system-dependent amplitudes related to the two system-dependent amplitudes in Eq. (1), while b^2 is a universal constant which is often approximated by [55]

$$b^2 = \frac{2-\alpha-4\beta}{(2-\alpha-2\beta)(1-2\beta)} \simeq 1.361. \tag{23}$$

Equations (20) and (22) with the specific choice (23) for b^2 is known as the "restricted" linear model [47]. The resulting parametric equations for the various thermodynamic properties can be found in many publications [47–49,51,56,57]. The parametric equations needed for the analysis in this report are listed in Appendix A.

5 Comparison with experimental data

The liquid–liquid transition (LLT) curve that follows from Eq. (10) is a straight line, in contrast to the LLT curves in Fig. 8. We consider a curved LLT to be more realistic than a straight line, but curvature in the scaled model (e.g., due to a pressure-dependent a') yields terms proportional to ϕ_1 in one or more response functions. Unlike the scaling susceptibilities, ϕ_1 does not vanish far away from the critical point, where the critical part should not play any role. A phenomenological attempt to include curvature of the LLT curve has been made by Fuentevilla and Anisimov [6]. However, it is not yet clear how to include such a curvature systematically into the theory.

Table 1: Parameter values for the model of Sec. 5

Parameter	Value	Parameter	Value
T_c/K	224.22	c_{12}	−0.007 896 9
P_c/MPa	27.500	c_{13}	0.009 088 2
$\rho_c/(\mathrm{kg\,m^{-3}})$	948.55	c_{14}	−0.000 450 23
a	0.233 49	c_{20}	−3.889 9
k	0.377 13	c_{21}	0.177 93
a'	0.090 000	c_{22}	−0.063 409
c_{02}	0.073 630	c_{23}	−0.007 515 0
c_{03}	−0.000 627 73	c_{30}	0.698 64
c_{04}	−0.001 088 2	c_{31}	−0.126 39
c_{05}	0.000 319 55	c_{32}	0.075 590
c_{11}	0.153 82	c_{41}	0.009 873 1

As Fig. 8 shows, the LLT curve cannot be accurately represented by a single straight line in the entire pressure range. We have, therefore, restricted the range of our model to pressures up to 150 MPa. Furthermore, the slope of the LLT line was constrained to values that are close to the slopes of the curves of Kanno and Angell [18] and Mishima [13] in the range of 0 MPa to 150 MPa. Specifically, the value of a' in Eq. (10) was restricted to the range of 0.065 to 0.090. Because the position of the LLT is not precisely known, the critical point was allowed to deviate up to 3 K from Mishima's curve. During the fitting process, it was found that the results of the model were quite insensitive to the critical pressure P_c. For that reason, P_c was constrained to the value of 27.5 MPa obtained by Bertrand and Anisimov [3]. It was also found that a nonzero mixing coefficient b' did not significantly improve the fit, so b' was set to zero. This means physically that the liquid-critical behavior in supercooled water exhibits little asymmetry in the order parameter.

Changes in the third decimal place of the values of the critical exponents α and β result in small density changes that are of the order of 0.1%. However, some of the density measurements for water are more accurate than 0.1%; for example, the accuracy of the data of Hare and Sorensen [15] and Sotani et al. [14] is 0.01%. Therefore, the values of the critical exponents must be given with at least four decimal places. We have adopted the values of Pelissetto and Vicari [41] and have set $\alpha = 0.1100$ and $\beta = 0.3265$. The values for the molar mass of H_2O (18.015 268 g/mol) and the ideal-gas constant R ($8.314\,472\ \mathrm{J\,mol^{-1}\,K^{-1}}$) were taken from Wagner and Pruß [11].

The number of terms in the background $\Delta\hat{\mu}^{\mathrm{r}}$ [Eq. (14)] was increased step by step until the experimental data could be represented. The final background contains sixteen free parameters. The reason for the many background terms of higher order in temperature and pressure is that the response functions are second derivatives of the thermodynamic potential. To obtain, for example, a background term in the heat capacity of second order in temperature, it is necessary to have a fourth-order temperature-dependent term in the potential. The terms in the backgrounds for each property are at most third order in temperature or in pressure.

Besides the background parameters, there are five additional parameters to be determined: the critical temperature T_c and volume V_c, the linear-model amplitudes a and k, and the slope of the LLT line a'. As noted, the values of T_c and a' were constrained to a limited range.

The model was fitted to heat-capacity data of Archer and Carter [31] and IAPWS-95, expansivity data of Hare and Sorensen [15], IAPWS-95 and Ter Minassian [16], compressibility data of Speedy and Angell [20], Kanno and Angell [18] and Mishima [13], and density data of Hare and Sorensen [15], Sotani et al. [14], IAPWS-95 and Mishima [13]. For all quantities except the heat capacity, values calculated from IAPWS-95 were only used at 0.1 MPa. (As noted in Section 3.3, values of IAPWS-95 replace the high-pressure heat-capacity data of Sirota et al. [33].) To reduce the time needed for optimization, not all data points were used in the fitting process; about 60 points were selected for each of the four quantities. The locations of the selected points are shown in Fig. 9.

The deviation of the model from an experimental data point is measured by the

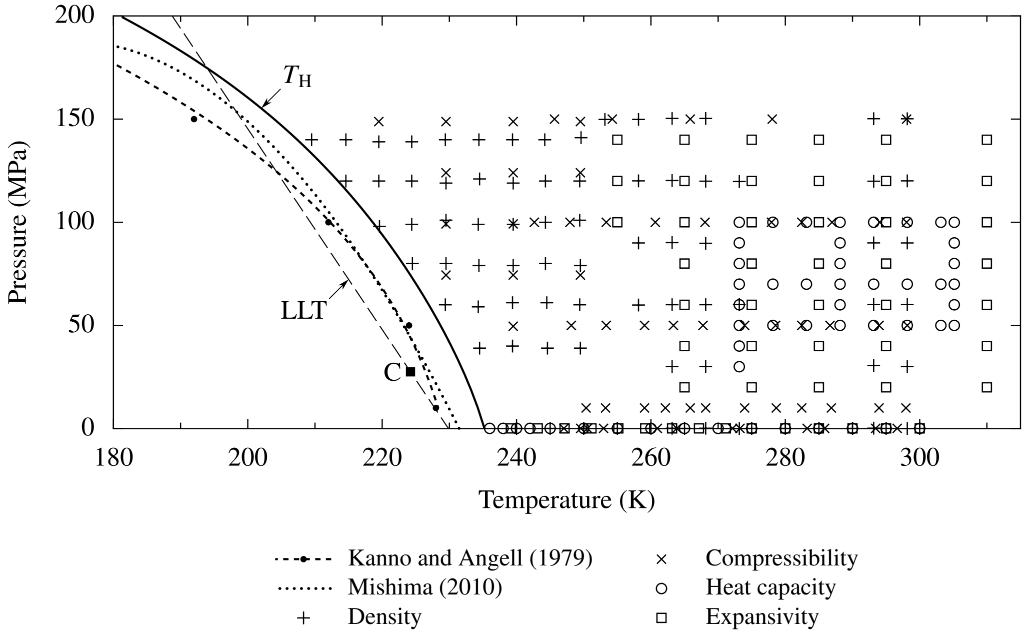

Figure 9: Location of experimental data points used for the fit of the model (plus, cross, circle, and square symbols). The solid curve marks the homogeneous nucleation limit. The long-dashed line marked by LLT is the model's liquid–liquid transition line and Widom line, with the critical point denoted by C. Also shown are the curves of Kanno and Angell [18] and Mishima [13].

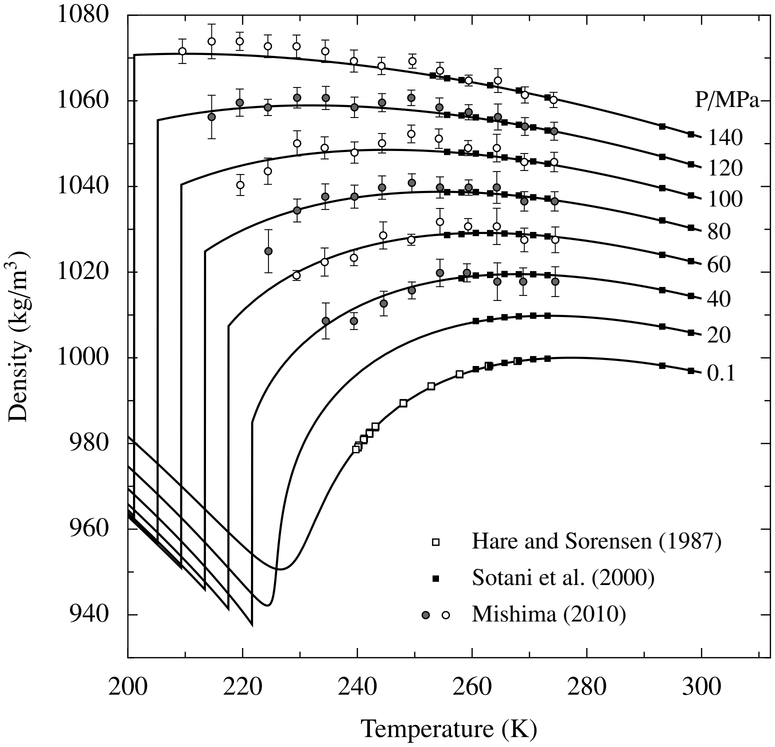

Figure 10: Densities according to the model (curves). The symbols represent experimental data of Mishima [13], Sotani et al. [14] and Hare and Sorensen [15]. The symbols for Mishima's densities on different isobars are alternatingly open and filled to guide the eye.

relative residual [58]

$$\frac{q_n^{\text{model}} - q_n^{\text{expt}}}{\sigma_{q,n}}, \tag{24}$$

where q_n is data point number n of property q, 'model' refers to the value calculated from the model and 'expt' refers to the experimental value. The residual is scaled by the experimental uncertainty $\sigma_{q,n}$ of that particular data point. For some data the uncertainty was not given and had to be estimated. The model was optimized by minimizing the sum of squared residuals; more precisely, the reduced chi-squared statistic

$$\chi^2_{\text{red}} = \frac{1}{N}\sum_{n=1}^{N}\left(\frac{q_n^{\text{model}} - q_n^{\text{expt}}}{\sigma_{q,n}}\right)^2 \tag{25}$$

was minimized, where N is the number of data points. It should be noted that the χ^2_{red} computed here cannot be used to assess the quality of the fit in a statistically rigorous way, because the true χ^2_{red} cannot be computed for nonlinear models [59].

The optimized parameters are listed in Table 1. The value of a' is exactly 0.09 because a' was restricted to the range of 0.065 to 0.090, and the optimum is located at the edge of this range.

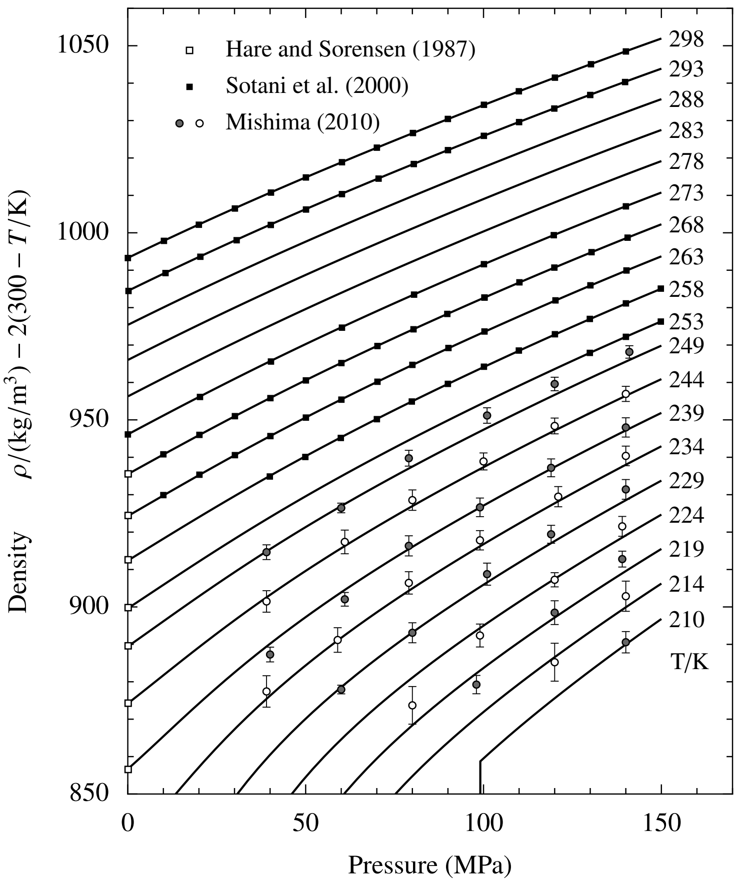

Figure 11: Densities according to the model (curves). The symbols represent experimental data of Mishima [13], Sotani et al. [14] and Hare and Sorensen [15]. The symbols for Mishima's densities on different isotherms are alternatingly open and filled to guide the eye. To prevent overlap, the densities for different temperatures have been shifted vertically by 2 kg $\mathrm{m}^{-3} \times (T/\mathrm{K} - 300)$.

The model is compared with density data in Figs. 10 and 11. The model represents the data well. The difference between some of Mishima's data points and the model is larger than the error bars, but this could be caused by an underestimation of the uncertainties by Mishima. In Fig. 10, the density jumps at low temperature because the isobars cross the LLT curve there.

In Fig. 12, the temperature of maximum density is plotted as a function of pressure, both for the model and for the IAPWS-95 formulation. At pressures higher than about 60 MPa, the values of IAPWS-95 deviate from the experimental data, while the current model agrees with the data. At negative pressures, the model does not agree with the experimental data, but the model was not fitted to any data at negative pressures, and negative pressures are not in the range of validity of the current model.

Compressibility data are compared with values of the model in Fig. 13. The iso-

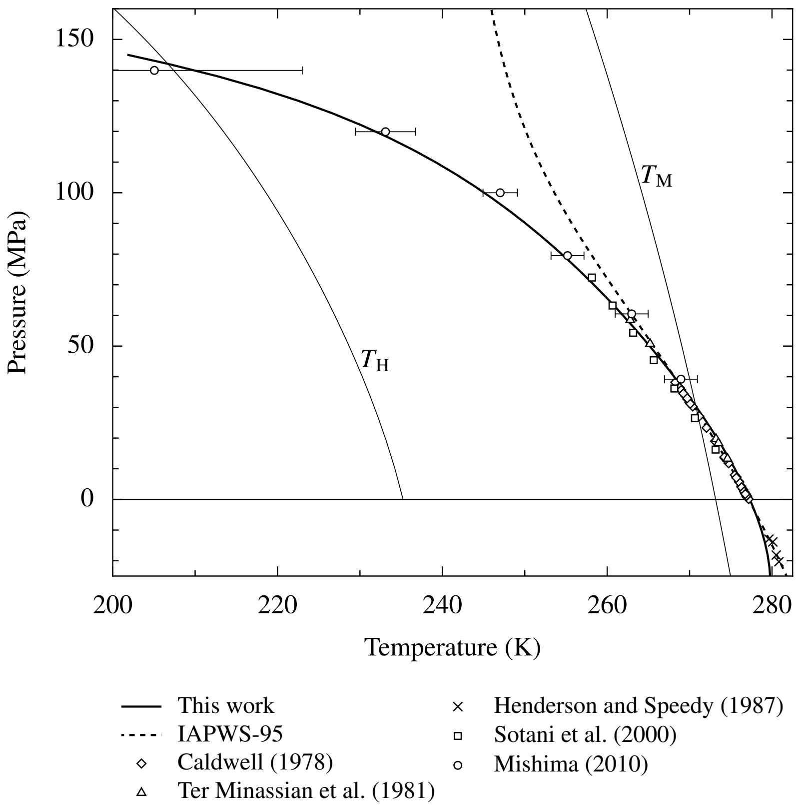

Figure 12: Temperature of maximum density as a function of pressure according to the model (thick solid curve) and IAPWS-95 (dashed curve). T_M marks the melting curve [24] and its extension to negative pressures [60]; T_H denotes the homogeneous nucleation limit [21]. Symbols represent experimental data [13,14,16,61,62]. The temperatures of maximum density for Mishima's data [13] were determined by locating the maxima of fits to his density data.

bars of 0.1 MPa and 10 MPa intersect at about 253 K. The experimental data do not confirm or rule out such an intersection because of the scatter and the lack of data below 245 K. However, the intersection implies that the pressure derivative of the compressibility, $(\partial \kappa_T/\partial P)_T$, is positive at low temperature and ordinary pressures.

Figure 14 shows experimental data for the expansivity coefficient and the values predicted by the model for five pressures. The model follows the experimental data, contrary to the IAPWS-95 formulation. At 240 K, where the difference between Hare and Sorensen's data of 1986 and 1987 is largest, the expansivity predicted by the model lies between them.

Heat-capacity data are compared with the model's predictions in Figs. 15 and 16. In Fig. 15, it is seen that the model follows the data of Archer and Carter [31], whereas IAPWS-95 follows the data of Angell et al. [30], to which it was fitted. However, the curvature of the 0.1 MPa isobar of the model is slightly higher than that suggested by the data of Archer and Carter. Murphy and Koop [63] proposed a heat capacity curve with a broader peak than that of our model, but with about the same maximum value. Figure 16 shows the heat capacity as a function of pressure. As mentioned in Section 3.3, there is a systematic difference between the data of Sirota et al. [33] and the values of IAPWS-95, and the data of Sirota et al. were not selected for the fit of the current model. At 250 K and pressures above about 50 MPa, the model predicts a smaller pressure dependence of the heat capacity than IAPWS-95. The pressure dependence of the heat capacity is thermodynamically related to the expansivity coefficient, and we have seen that the expansivity coefficient of IAPWS-95 does not agree with experimental data at low temperature and high pressure (see Fig. 14). Therefore, differences between the heat-capacity values of the current model and IAPWS-95 are to be expected.

To analyze the quality of the model more extensively, residuals have been calculated for all available experimental data points in the range of validity, not just those selected for fitting. Figure 17 shows that the residuals are roughly normally distributed.

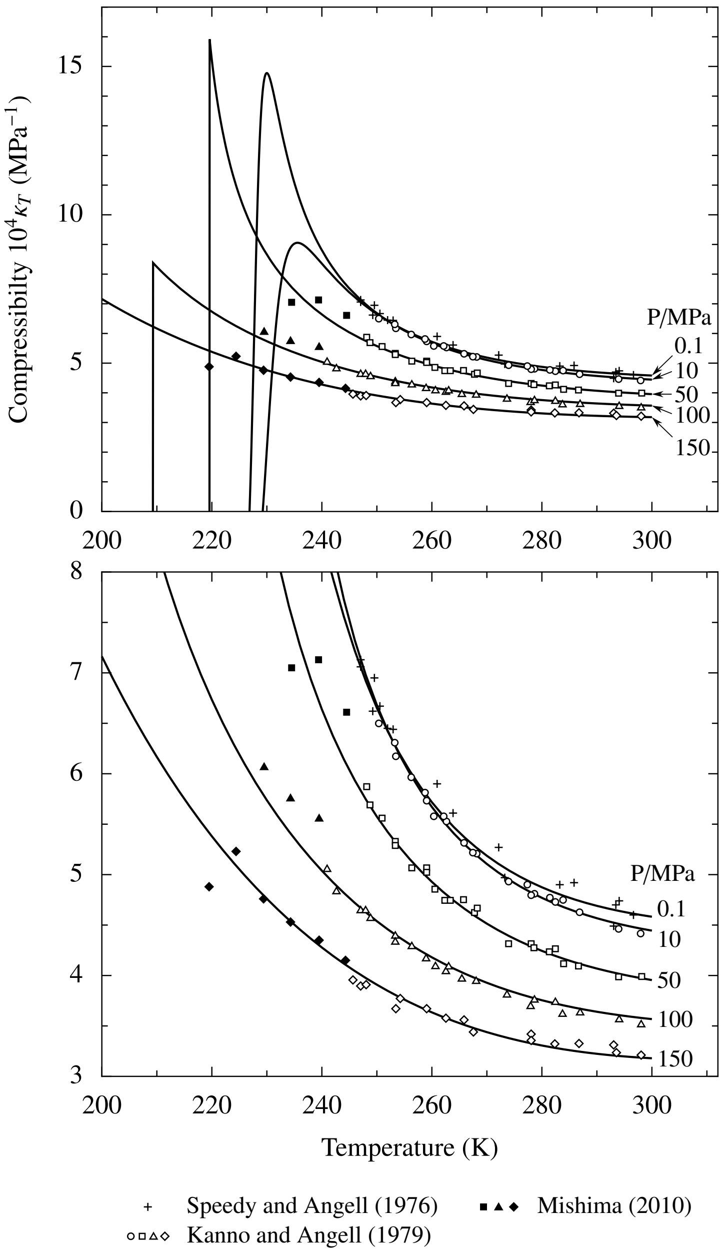

Figure 13: Isothermal compressibility according to the model (curves). For clarity, the curves are not shown for temperatures below the LLT line in the bottom graph. Symbols represent experimental data of Speedy and Angell [20], Kanno and Angell [18], and Mishima [13]. Solid and open symbols with the same shape correspond to the same pressure.

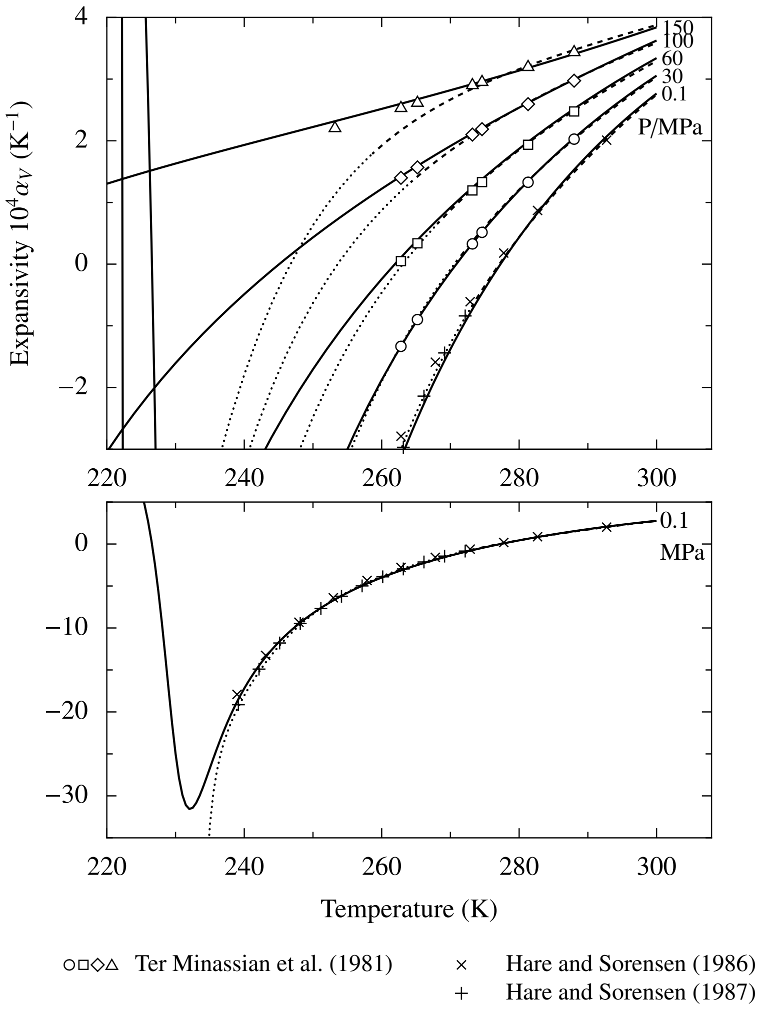

Figure 14: Expansivity coefficient according to the model (solid curves) and IAPWS-95 (dashed: within region of validity, dotted: extrapolations). Symbols represent experimental data of Ter Minassian et al. [16] and Hare and Sorensen [15,17].

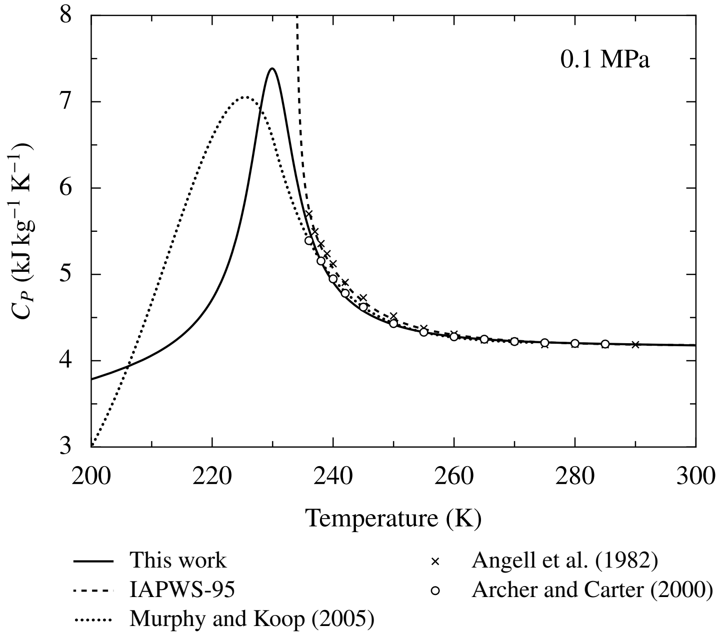

Figure 15: Isobaric heat capacity versus temperature according to the model (solid curve), IAPWS-95 (dashed), and Murphy and Koop (dotted). Symbols represent experimental data of Angell et al. [30] and Archer and Carter [31].

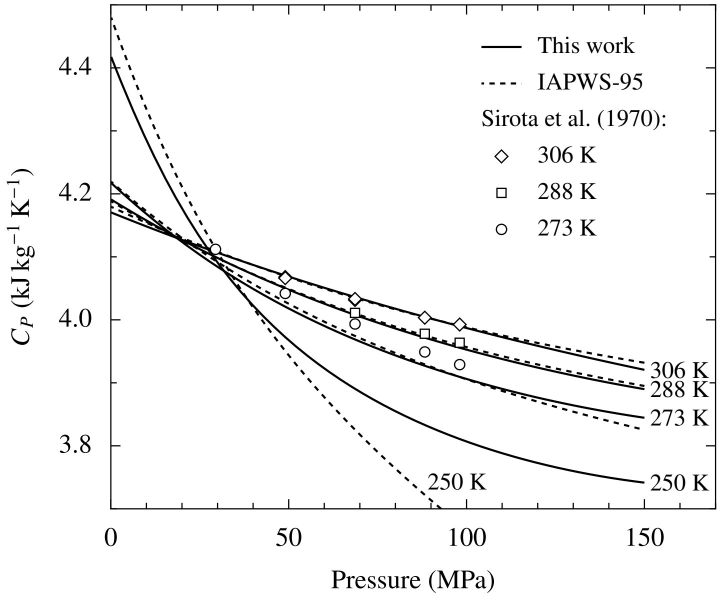

Figure 16: Isobaric heat capacity versus pressure according to the model (solid curves) and IAPWS-95 (dashed). Symbols represent experimental data of Sirota et al. [33].

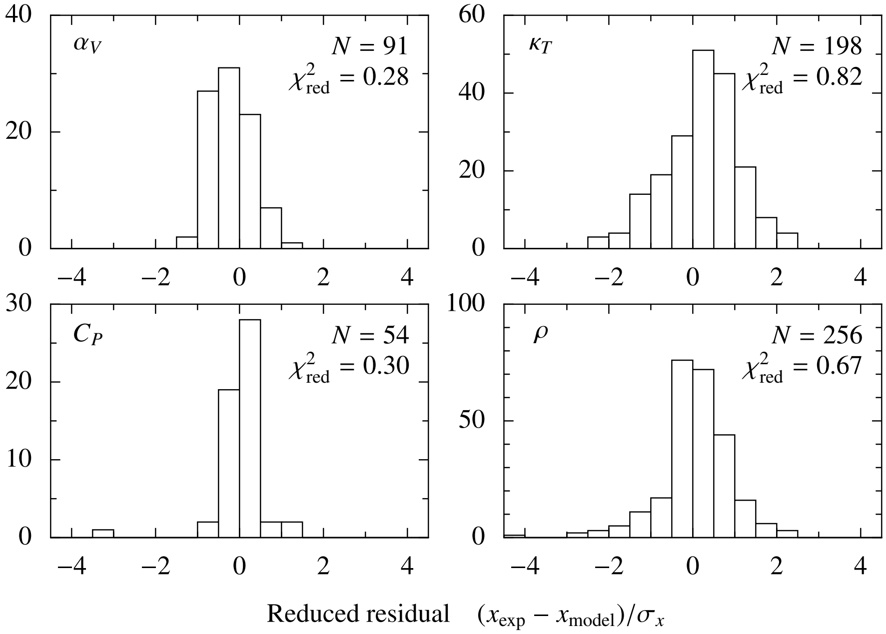

Figure 17: Histograms of reduced residuals [Eq. (24)] of the four quantities. In each graph, N indicates the number of data points and χ^2_{red} is the reduced chi-squared [Eq. (25)].

6 Phenomenological extension of thermodynamic model

If the LLT line is allowed to deviate more from the expected location, almost all experimental data up to 400 MPa can be represented. The constraint that the critical point should be at most 3 K from Mishima's LLT curve was removed. In addition, the slope of the LLT line and the critical pressure were not constrained. With these constraints removed, it was possible to fit all experimental data with the model equation without the addition of any parameters.

The model was fitted to a selection of experimental data at pressures up to 400 MPa which is shown in Fig. 18. The resulting parameters are listed in Table 2. The critical pressure is about a factor of two higher than in the previous section.

A comparison between the density values predicted by the model is presented in Figs. 19 and 20. The model reproduces most of the data, except Mishima's points between 160 MPa and 300 MPa below 230 K. The temperature of maximum density is plotted in Fig. 21. The results of the model are similar to those of the previous section (Fig. 12) in the range from 0 MPa to 120 MPa. At higher pressures, the extended model predicts significantly higher temperatures of maximum density than the previous model, but the results are still within the experimental uncertainty. At negative pressures, the extended model performs better than the previous model.

Compressibility data are compared with values of the model in Fig. 22. As in the previous model, the isobars of 0.1 MPa and 10 MPa intersect, but the intersection is located at a lower temperature. The data of Speedy and Angell [20] and Kanno and Angell [18] are well represented. The model does not reproduce all of Mishima's data, but these data have a lower accuracy than the data of Angell and coworkers.

Figure 23 shows the expansivity coefficient predicted by the extended model. Below 250 K, the model agrees better with the data of Hare and Sorensen of 1986 than with their data of 1987.

Table 2: Parameter values for the model of Sec. 6

Parameter	Value	Parameter	Value
T_c/K	214.175	c_{12}	-1.89496×10^{-3}
P_c/MPa	57.7658	c_{13}	2.11483×10^{-3}
$\rho_c/(\mathrm{kg\,m^{-3}})$	955.225	c_{14}	-2.82538×10^{-4}
a	0.121158	c_{20}	-3.65173
k	0.393246	c_{21}	-3.57012×10^{-3}
a'	0.113638	c_{22}	-2.78849×10^{-2}
c_{02}	3.75419×10^{-2}	c_{23}	1.22032×10^{-3}
c_{03}	-6.57463×10^{-4}	c_{30}	5.60699×10^{-1}
c_{04}	1.73555×10^{-5}	c_{31}	1.01406×10^{-1}
c_{05}	7.73226×10^{-6}	c_{32}	1.40791×10^{-2}
c_{11}	1.78841×10^{-1}	c_{41}	-7.85536×10^{-2}

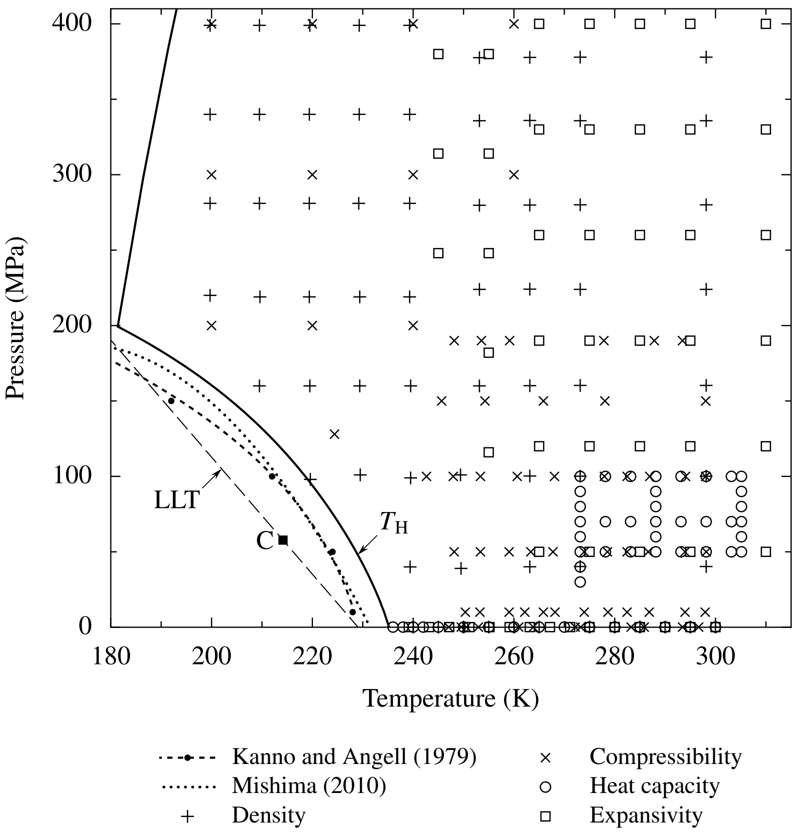

Figure 18: Location of experimental data points used for the fit of the model (plus, cross, circle, and square symbols). The solid curve marks the homogeneous nucleation limit. The long-dashed line marked by LLT is the model's liquid–liquid transition line and Widom line, with the critical point denoted by C. Also shown are the curves of Kanno and Angell [18] and Mishima [13].

The calculated heat capacity at 0.1 MPa is compared with experimental data in Fig. 24. For this model, the maximum of the heat capacity is lower than for the previous model. The curvature of the data of Archer and Carter [31] is better represented than previously, but there is still a systematic difference between their data and the model's results. The heat capacity is shown as a function of pressure in Fig. 25. There are large differences between the results of the model and those of IAPWS-95; the model predicts a minimum in the 250 K heat-capacity isotherm at about 240 MPa. A minimum in the heat capacity at this location was also predicted by Ter Minassian et al. [16] based on their measurements of the expansivity coefficient.

Figure 26 shows histograms of the reduced residuals of each quantity, calculated for all available data points, not just those selected for fitting. It is seen that the distributions are broader than those of the model of the previous section. The tails of the compressibility and density histograms indicate that the model does not represent all experimental points. Some compressibility data points of Mishima [13] at

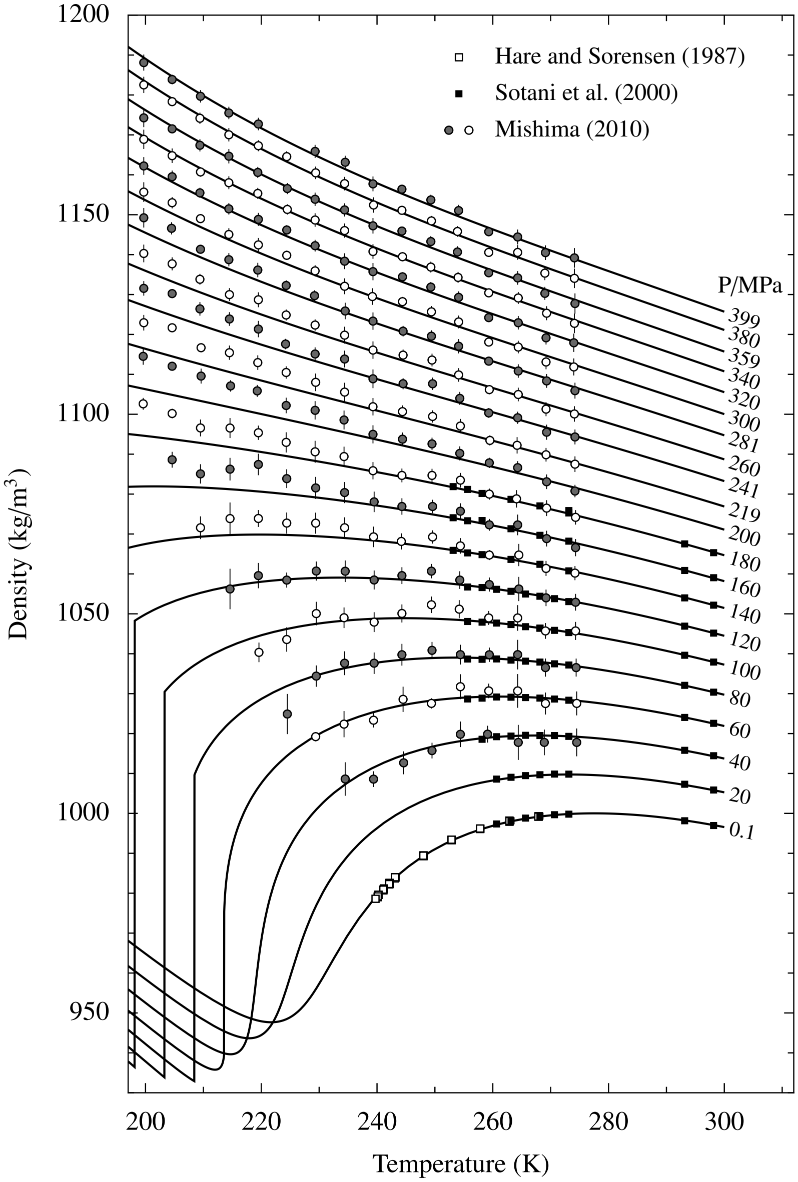

Figure 19: Densities according to the model (curves). The symbols represent experimental data of Mishima [13], Sotani et al. [14] and Hare and Sorensen [15]. The symbols for Mishima's densities on different isobars are alternatingly open and filled to guide the eye. The vertical lines through Mishima's points are uncertainties given by Mishima.

200 K and 205 K between 200 MPa and 350 MPa show deviations of about 20% from the values calculated by the model. However, since Mishima did not specify the accuracy of his compressibility measurements, the significance of the deviation is unknown. In the case of the density, several low-temperature measurements of Mishima [13] differ up to about 0.7% from the values computed by the model as shown in Figs. 19 and 20.

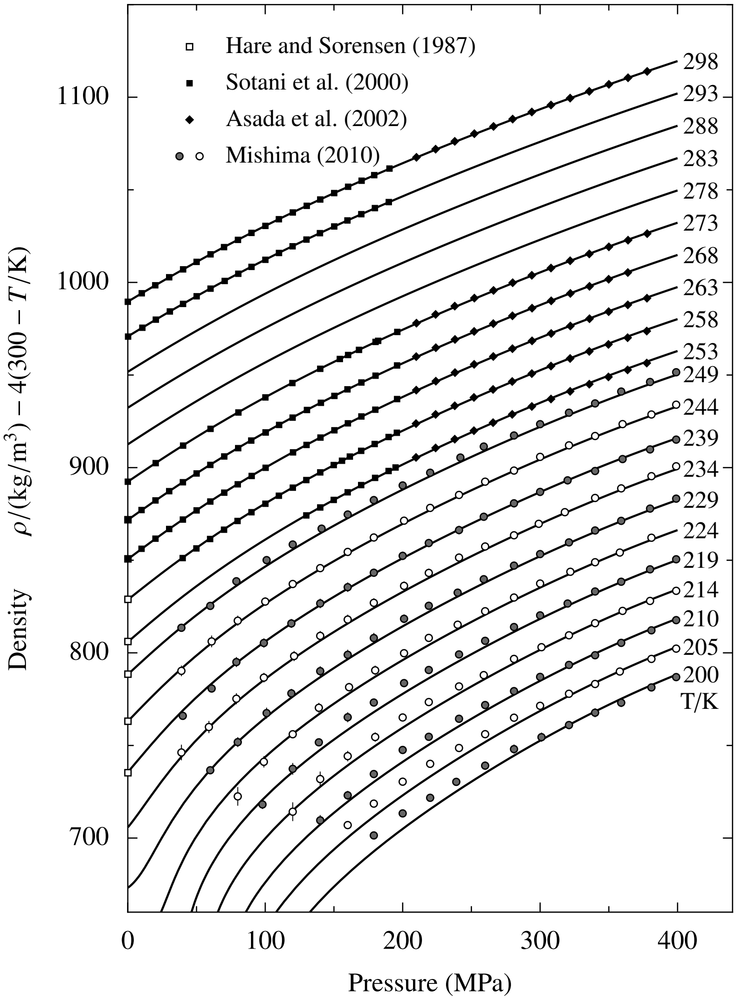

Figure 20: Densities according to the model (curves). The symbols represent experimental data of Mishima [13], Sotani et al. [14] and Hare and Sorensen [15]. The symbols for Mishima's densities on different isotherms are alternatingly open and filled to guide the eye. To prevent overlap, the densities for different temperatures have been shifted vertically by 4 kg $\mathrm{m}^{-3} \times (T/\mathrm{K} - 300)$.

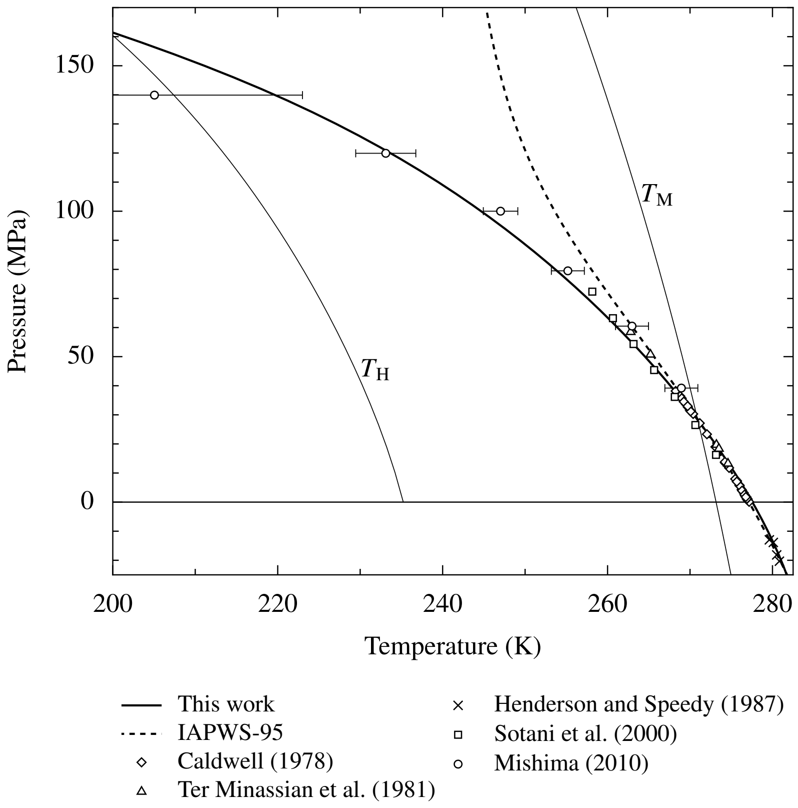

Figure 21: Temperature of maximum density as a function of pressure according to the model (thick solid curve) and IAPWS-95 (dashed curve). T_M marks the melting curve [24] and its extension to negative pressures [60]; T_H denotes the homogeneous nucleation limit [21]. Symbols represent experimental data [13,14,16,61,62]. The temperatures of maximum density for Mishima's data [13] were determined by locating the maxima of fits to his density data.

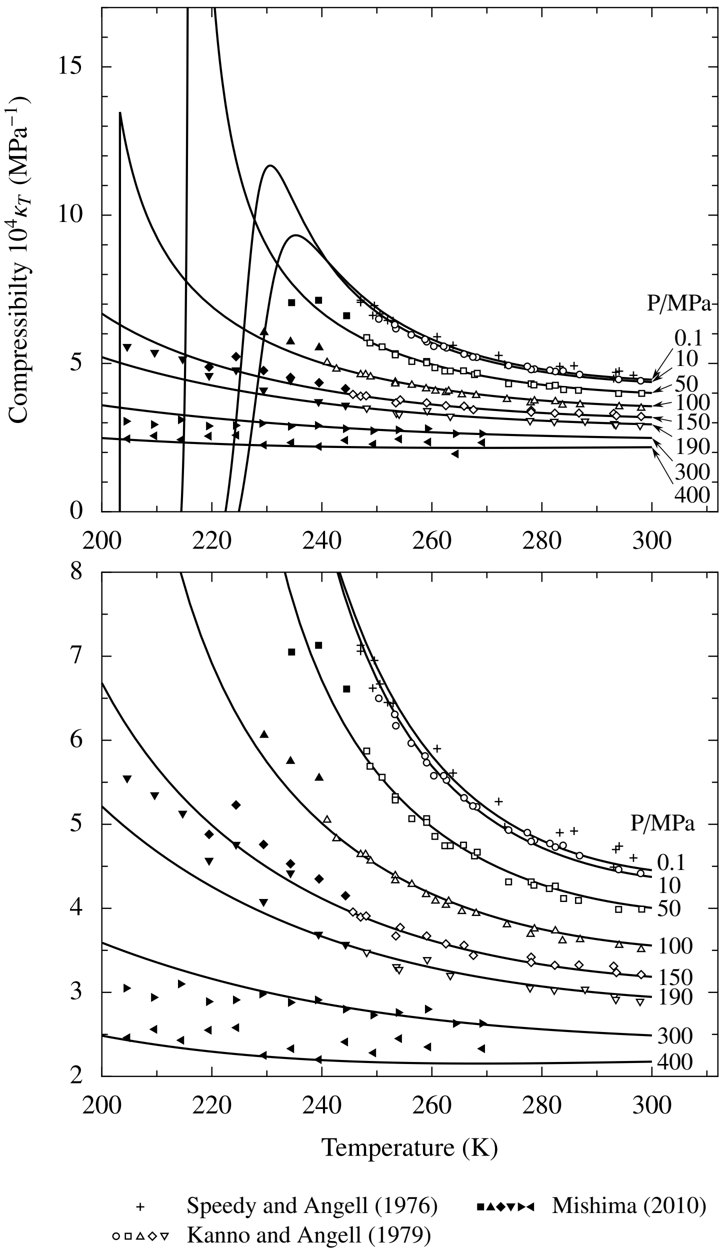

Figure 22: Isothermal compressibility according to the model (curves). For clarity, the curves are not shown for temperatures below the LLT line in the bottom graph. Symbols represent experimental data of Speedy and Angell [20], Kanno and Angell [18], and Mishima [13]. Solid and open symbols with the same shape correspond to the same pressure.

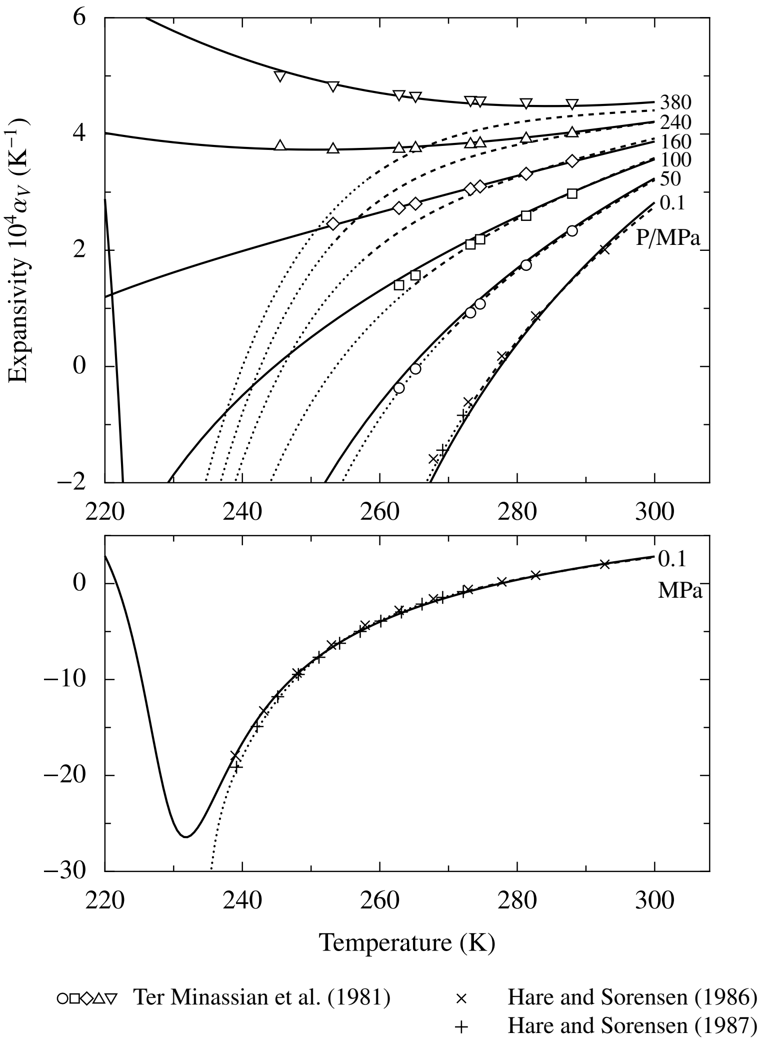

Figure 23: Expansivity coefficient to the model (solid curves) and IAPWS-95 (dashed: within region of validity, dotted: extrapolations). Symbols represent experimental data of Ter Minassian et al. [16] and Hare and Sorensen [15,17].

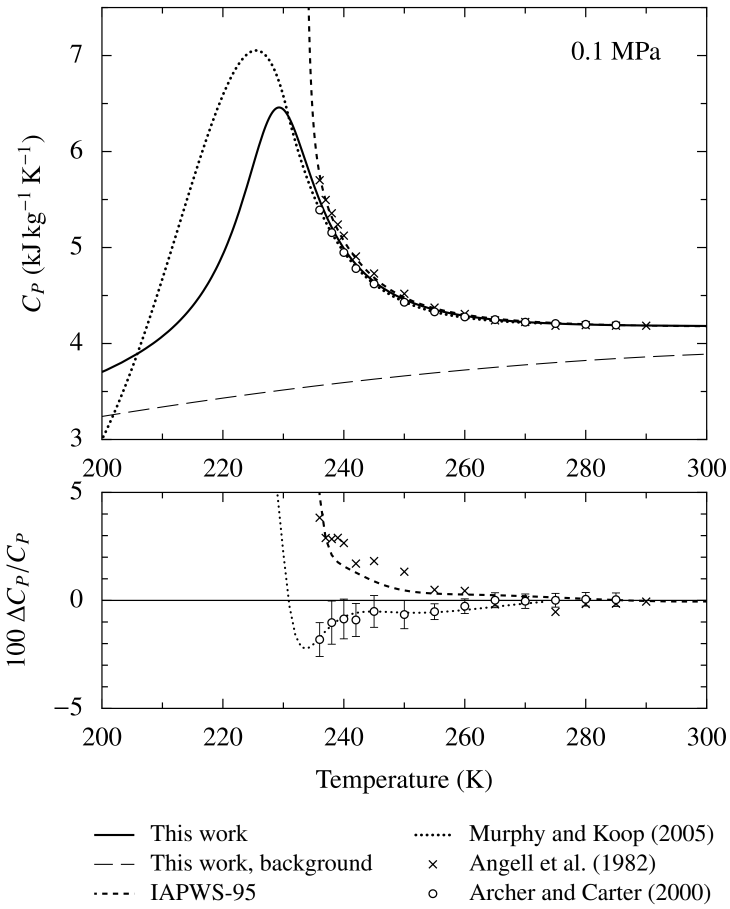

Figure 24: Isobaric heat capacity versus temperature according to the model (solid curve), IAPWS-95 (short dashed), and Murphy and Koop (dotted). The background contribution of the model is shown by the long-dashed curve. Symbols represent experimental data of Angell et al. [30] and Archer and Carter [31]. The bottom graph shows the relative difference, $100\Delta C_P/C_P = 100(C_P^{\text{exp}} - C_P^{\text{model}})/C_P^{\text{model}}$, between experimental data and values calculated by the model.

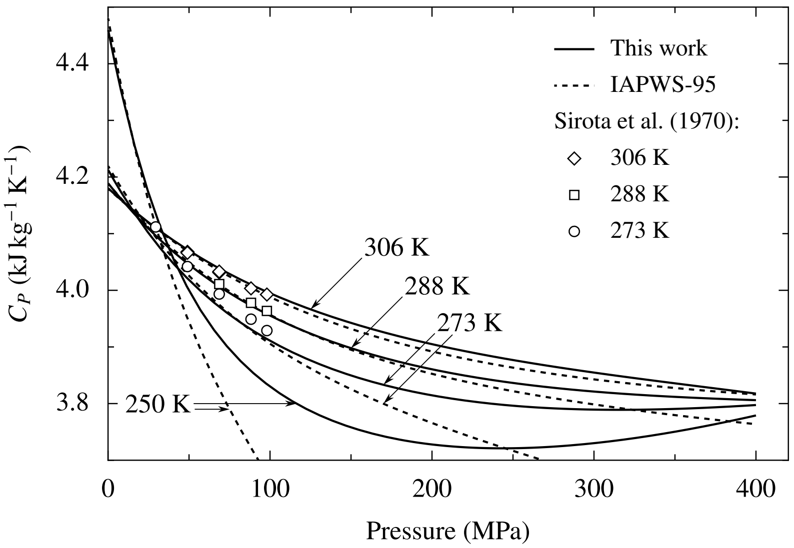

Figure 25: Isobaric heat capacity versus pressure according to the model (solid curves) and IAPWS-95 (dashed). Symbols represent experimental data of Sirota et al. [33].

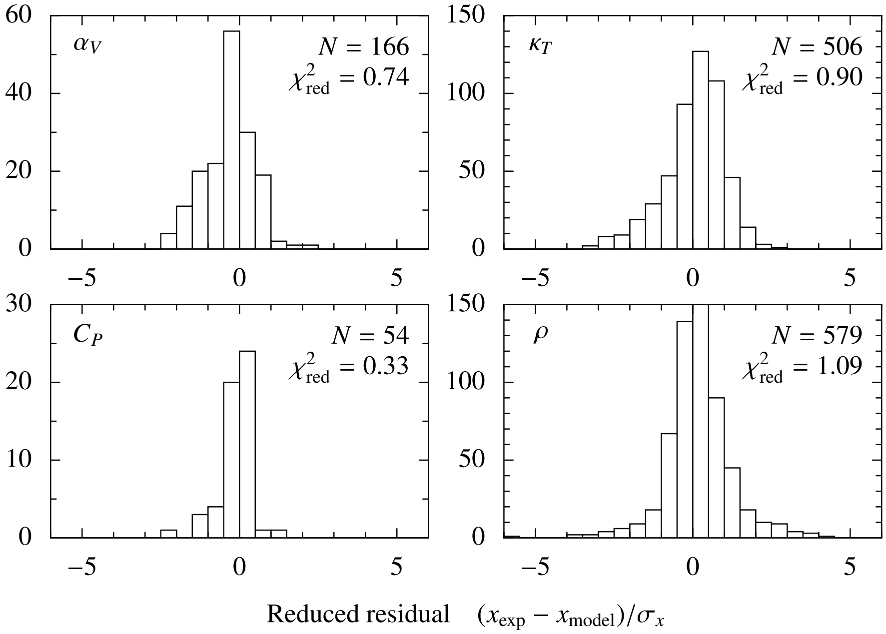

Figure 26: Histograms of reduced residuals [Eq. (24)] of the four quantities. In each graph, N indicates the number of data points and χ^2_{red} is the reduced chi-squared [Eq. (25)].

7 Discussion

We have seen that a theoretical model based on the assumption of a liquid–liquid critical point in supercooled water can represent the thermodynamic properties of supercooled water to pressures of 150 MPa. Moreover, by allowing the slope of the liquid–liquid transition (LLT) line and the critical pressure to be freely adjustable parameters the model can represent almost all available thermodynamic property data for supercooled water. Nevertheless, there are still a number of issues that need to be considered.

First, the theoretical model for critical behavior assumes that the LLT curve is a straight line as a function of pressure or temperature. While the precise location of the LLT curve is somewhat uncertain, it is likely to be curved. Fuentevilla and Anisimov [6] have made an attempt to incorporate such a curvature by adding a quadratic pressure term to the expression (10) for the ordering field. However, it is not yet clear how the expansions (10)–(12) for the scaling fields can be generalized to include higher-order contributions from the physical fields in a thermodynamically consistent way. Another possibility for extending the range of validity of the theoretical model may be to account for a crossover from Ising-like fluctuation-induced critical behavior asymptotically close to the liquid–liquid critical point to classical mean-field behavior farther away from the critical point, as has been done in the representation of the thermodynamic properties of H_2O in a wide range of temperatures and densities around its vapor–liquid critical point [64] and has also been suggested by Kiselev [4,5].

The existence of a liquid–liquid critical point is not the only possible explanation for the anomalous behavior of the thermodynamic properties of supercooled water. Scenarios for a singularity-free or critical-point-free interpretation have been proposed [65–67]. Another suggestion is that response functions like the compressibility do not diverge at a single temperature corresponding to a critical temperature but at a range of pressure dependent temperatures $T_\mathrm{S}(P)$ corresponding to a spinodal instability [18,68,69]. Most recently, the discussion on the nature of the anomalies observed in supercooled water has received an additional impetus after Limmer and Chandler reported new simulation results [8] for two atomistic models of water, mW [70] and mST2 [71]. They found only a single liquid state in the supercooled region and excluded the possibility of the liquid-critical point for the models studied. It would be important to compare the anomalies predicted by the models with those exhibited by real water. The final conclusion on the existence of the liquid–liquid critical point in water should be based on the ability to quantitatively describe the experimental data.

The information provided in this report shows that a critical-point parametric equation of state describes the available thermodynamic data on supercritical water within experimental accuracy, thus establishing a benchmark for any further developments in this area.

Acknowledgments

The research of V. Holten at the University of Maryland has been supported by the Burgers Program of the University of Maryland (four months). The research of C. E. Bertrand and one month of V. Holten has been supported by the Division of Chemistry of the US National Science Foundation under Grant No. CHE-1012052. Travel support for V. Holten was provided by the J. M. Burgerscentrum in the Netherlands.

Appendix A Linear-model parametric equations

The formulas for the linear model are from Behnejad et al. [49].*

The r and θ coordinates are related to h_1 and h_2 by

$$h_1 = a r^{\beta+\gamma}\theta(1-\theta^2), \tag{26}$$

$$h_2 = r(1-b^2\theta^2), \tag{27}$$

with $\gamma = 2-\alpha-2\beta$ and

$$b^2 = \frac{\gamma-2\beta}{\gamma(1-2\beta)}. \tag{28}$$

The scaling densities are given by

$$\phi_1 = k r^{\beta}\theta \tag{29}$$

$$\phi_2 = a k r^{1-\alpha} s(\theta), \tag{30}$$

with

$$s(\theta) = L_0(s_0 + s_2\theta^2), \tag{31}$$

$$L_0 = 1/[2b^4(1-\alpha)\alpha], \tag{32}$$

$$s_0 = (\gamma-2\beta) - b^2\alpha\gamma, \tag{33}$$

$$s_2 = (\alpha-1)(\gamma-2\beta)b^2. \tag{34}$$

The scaling susceptibilities are given by

$$\chi_1 = \frac{k}{a} r^{-\gamma} q_1(\theta), \tag{35}$$

$$\chi_{12} = k r^{\beta-1} q_{12}(\theta), \tag{36}$$

$$\chi_2 = a k r^{-\alpha} q_2(\theta), \tag{37}$$

---

* In Behnejad et al. [49], the formula corresponding to our Eq. (40) erroneously does not contain the factor L_0.

with

$$q_1(\theta) = (1 - b^2\theta^2 + 2\beta b^2\theta^2)/q_0(\theta), \tag{38}$$

$$q_{12}(\theta) = \theta[-\gamma + (\gamma - 2\beta)\theta^2]/q_0(\theta), \tag{39}$$

$$q_2(\theta) = [(1-\alpha)(1-3\theta^2)s(\theta) - (\beta+\gamma)2s_2L_0\theta^2(1-\theta^2)]/q_0(\theta), \tag{40}$$

$$q_0(\theta) = (1-3\theta^2)(1-b^2\theta^2) + 2b^2(\beta+\gamma)\theta^2(1-\theta^2). \tag{41}$$

References

1. P. G. Debenedetti, Supercooled and glassy water, *J. Phys.: Condens. Matter* **15**, R1669 (2003).
2. P. H. Poole, F. Sciortino, U. Essmann, and H. E. Stanley, Phase behaviour of metastable water, *Nature (London)* **360**, 324 (1992).
3. C. E. Bertrand and M. A. Anisimov, The peculiar thermodynamics of the second critical point in supercooled water, *J. Phys. Chem. B* (2011), in press (doi: 10.1021/jp204011z).
4. S. B. Kiselev, Physical limit of stability in supercooled liquids, *Int. J. Thermophys.* **22**, 1421 (2001).
5. S. B. Kiselev and J. F. Ely, Parametric crossover model and physical limit of stability in supercooled water, *J. Chem. Phys.* **116**, 5657 (2002).
6. D. A. Fuentevilla and M. A. Anisimov, Scaled equation of state for supercooled water near the liquid-liquid critical point, *Phys. Rev. Lett.* **97**, 195702 (2006), erratum ibid. **98**, 149904 (2007).
7. J. Kalová and R. Mareš, Crossover equation and the vapor pressure of supercooled water, *Int. J. Thermophys.* **31**, 756 (2010).
8. D. T. Limmer and D. Chandler, The putative liquid-liquid transition is a liquid-solid transition in atomistic models of water, *arXiv:1107.0337v1 [cond-mat.stat-mech]* (2011).
9. K. T. Wikfeldt, A. Nilsson, and L. G. M. Pettersson, Spatially inhomogeneous bimodal inherent structure in simulated liquid water, *arXiv:1106.5038v1 [cond-mat.soft]* (2011).
10. *Revised Release on the IAPWS Formulation 1995 for the Thermodynamic Properties of Ordinary Water Substance for General and Scientific Use*, IAPWS (2009). http://www.iapws.org/relguide/IAPWS95-Rev.pdf
11. W. Wagner and A. Pruß, The IAPWS formulation 1995 for the thermodynamic properties of ordinary water substance for general and scientific use, *J. Phys. Chem. Ref. Data* **31**, 387 (2002).
12. R. Feistel, D. G. Wright, K. Miyagawa, A. H. Harvey, J. Hruby, D. R. Jackett, T. J. McDougall, and W. Wagner, Mutually consistent thermodynamic potentials for fluid water, ice and seawater: a new standard for oceanography, *Ocean Sci.* **4**, 275 (2008).
13. O. Mishima, Volume of supercooled water under pressure and the liquid-liquid critical point, *J. Chem. Phys.* **133**, 144503 (2010).

14. T. Sotani, J. Arabas, H. Kubota, and M. Kijima, Volumetric behaviour of water under high pressure at subzero temperature, *High Temp. High Pressures* **32**, 433 (2000).
15. D. E. Hare and C. M. Sorensen, The density of supercooled water. II. Bulk samples cooled to the homogeneous nucleation limit, *J. Chem. Phys.* **87**, 4840 (1987).
16. L. Ter Minassian, P. Pruzan, and A. Soulard, Thermodynamic properties of water under pressure up to 5 kbar and between 28 and 120°C. Estimations in the supercooled region down to −40 °C, *J. Chem. Phys.* **75**, 3064 (1981).
17. D. E. Hare and C. M. Sorensen, Densities of supercooled H_2O and D_2O in 25 μ glass capillaries, *J. Chem. Phys.* **84**, 5085 (1986).
18. H. Kanno and C. A. Angell, Water: Anomalous compressibilities to 1.9 kbar and correlation with supercooling limits, *J. Chem. Phys.* **70**, 4008 (1979).
19. S. Asada, T. Sotani, J. Arabas, H. Kubota, S. Matsuo, and Y. Tanaka, Density of water at subzero temperature under high pressure: measurements and correlation, *J. Phys.: Condens. Matter* **14**, 11447 (2002).
20. R. J. Speedy and C. A. Angell, Isothermal compressibility of supercooled water and evidence for a thermodynamic singularity at −45°C, *J. Chem. Phys.* **65**, 851 (1976).
21. H. Kanno, R. J. Speedy, and C. A. Angell, Supercooling of water to −92 °C under pressure, *Science* **189**, 880 (1975).
22. H. Kanno and K. Miyata, The location of the second critical point of water, *Chem. Phys. Lett.* **422**, 507 (2006).
23. P. G. Debenedetti, Reply to comment on 'Supercooled and glassy water', *J. Phys.: Condens. Matter* **16**, 6815 (2004).
24. *Revised Release on the Pressure along the Melting and Sublimation Curves of Ordinary Water Substance*, IAPWS (2008). http://www.iapws.org/relguide/meltsub.pdf
25. A. Saul and W. Wagner, A fundamental equation for water covering the range from the melting line to 1273 K at pressures up to 25 000 MPa, *J. Phys. Chem. Ref. Data* **18**, 1537 (1989).
26. G. S. Kell, Density, thermal expansivity, and compressibility of liquid water from 0° to 150°C: Correlations and tables for atmospheric pressure and saturation reviewed and expressed on 1968 temperature scale, *J. Chem. Eng. Data* **20**, 97 (1975).
27. IAPWS, file "p-rho-t-kell-1975.dat" (2006). http://www.iapws.org/95data.htm
28. M. A. Anisimov, A. V. Voronel', N. S. Zaugol'nikova, and G. I. Ovodov, Specific heat of water near the melting point and Ornstein–Zernike fluctuation corrections, *JETP Lett.* **15**, 317 (1972).
29. C. A. Angell, J. Shuppert, and J. C. Tucker, Anomalous properties of supercooled water. Heat capacity, expansivity, and proton magnetic resonance chemical shift from 0 to −38°, *J. Phys. Chem.* **77**, 3092 (1973).
30. C. A. Angell, M. Oguni, and W. J. Sichina, Heat capacity of water at extremes of supercooling and superheating, *J. Phys. Chem.* **86**, 998 (1982).
31. D. G. Archer and R. W. Carter, Thermodynamic properties of the NaCl + H_2O system. 4. Heat capacities of H_2O and NaCl(aq) in cold-stable and supercooled states, *J. Phys. Chem. B* **104**, 8563 (2000).

32. E. Tombari, C. Ferrari, and G. Salvetti, Heat capacity anomaly in a large sample of supercooled water, *Chem. Phys. Lett.* **300**, 749 (1999).
33. A. M. Sirota, A. J. Grishkov, and A. G. Tomishko, Experimental investigation of specific heat of water near fusion line, *Thermal Eng.* **17**, 90 (1970).
34. J. J. Manyà, M. J. Antal, Jr., C. K. Kinoshita, and S. M. Masutani, Specific heat capacity of pure water at 4.0 MPa between 298.15 and 465.65 K, *Ind. Eng. Chem. Res.* **50**, 6470 (2011).
35. O. Mishima and H. E. Stanley, Decompression-induced melting of ice IV and the liquid–liquid transition in water, *Nature* **392**, 164 (1998).
36. O. Mishima, Liquid-liquid critical point in heavy water, *Phys. Rev. Lett.* **85**, 334 (2000).
37. A. R. Imre and S. J. Rzoska, High-pressure melting curves and liquid–liquid phase transition, *Adv. Sci. Lett.* **3**, 527 (2010).
38. M. E. Fisher, Renormalization group in theory of critical behavior, *Rev. Mod. Phys.* **46**, 597 (1974).
39. L. P. Kadanoff, Scaling, universality and operator algebras, in *Phase Transitions and Critical Phenomena*, volume 5a, edited by C. Domb and M. S. Green (Academic Press, New York, 1976), pp. 1–34.
40. M. E. Fisher, Scaling, universality and renormalization group theory, in *Critical Phenomena, Lecture Notes in Physics*, volume 186, edited by F. J. W. Hahne (Springer, Berlin, 1983), pp. 1–139.
41. A. Pelissetto and E. Vicari, Critical phenomena and renormalization-group theory, *Phys. Rep.* **368**, 549 (2002).
42. J. V. Sengers and J. G. Shanks, Experimental critical-exponent values for fluids, *J. Stat. Phys.* **137**, 857 (2009).
43. J. S. Rowlinson and F. L. Swinton, *Liquids and Liquid Mixtures* (Butterworth, London, 1982), third edition.
44. M. A. Anisimov, E. E. Gorodetskii, V. D. Kulikov, and J. V. Sengers, Crossover between vapor-liquid and consolute critical phenomena, *Phys. Rev. E* **51**, 1199 (1995).
45. T. D. Lee and C. N. Yang, Statistical theory of equations of state and phase transitions. 2. Lattice gas and Ising model, *Phys. Rev.* **87**, 410 (1952).
46. M. E. Fisher, The theory of equilibrium critical phenomena, *Rep. Progr. Phys.* **30(II)**, 615 (1967).
47. J. V. Sengers and J. M. H. Levelt Sengers, Critical phenomena in classical fluids, in *Progress in Liquid Physics*, edited by C. A. Croxton (Wiley, New York, 1978), chapter 4, pp. 103–174.
48. J. M. H. Levelt Sengers, B. Kamgar-Parsi, F. W. Balfour, and J. V. Sengers, Thermodynamic properties of steam in the critical region, *J. Phys. Chem. Ref. Data* **12**, 1 (1983).
49. H. Behnejad, J. V. Sengers, and M. A. Anisimov, Thermodynamic behavior of fluids near critical points, in *Applied Thermodynamics of Fluids*, edited by A. R. H. Goodwin, J. V. Sengers, and C. J. Peters (RSC Publishing, Cambridge, UK, 2010), chapter 10, pp. 321–367.

50. M. A. Anisimov, S. B. Kiselev, J. V. Sengers, and S. Tang, Crossover approach to global critical phenomena in fluids, *Physica A* **188**, 487 (1992).

51. M.A. Anisimov, V.A. Agayan, and P.J. Collings, Nature of the Blue-Phase-III-isotropic critical point: An analogy with the liquid-gas transition, *Phys. Rev. E* **57**, 582 (1998).

52. M.E. Fisher, The theory of critical point singularities, in *Proceedings of the International school of Physics "Enrico Fermi"*, edited by M. S. Green (Academic Press, New York, 1971), pp. 1–99.

53. E. Brézin, D. J. Wallace, and K. G. Wilson, Feynman-graph expansion for the equation of state near the critical point (Ising-like case), *Phys. Rev. Lett.* **29**, 591 (1972).

54. P. Schofield, Parametric representation of the equation of state near a critical point, *Phys. Rev. Lett.* **22**, 606 (1969).

55. P. Schofield, J.D. Litster, and J.T. Ho, Correlation between critical coefficients and critical exponents, *Phys. Rev. Lett.* **23**, 1098 (1969).

56. P.C. Hohenberg and M. Barmatz, Gravity effects near the gas-liquid critical point, *Phys. Rev. A* **6**, 289 (1972).

57. M.R. Moldover, J.V. Sengers, R.W. Gammon, and R.J. Hocken, Gravity effects in fluids near the gas-liquid critical point, *Rev. Mod. Phys.* **51**, 79 (1979).

58. E. W. Lemmon and R. Span, Multi-parameter equations of state for pure fluids and mixtures, in *Applied Thermodynamics of Fluids*, edited by A. R. H. Goodwin, J. V. Sengers, and C. J. Peters (RSC Publishing, Cambridge, UK, 2010), chapter 12, pp. 394–432.

59. R. Andrae, T. Schulze-Hartung, and P. Melchior, Dos and don'ts of reduced chi-squared, *arXiv:1012.3754v1 [astro-ph.IM]* (2010).

60. S.J. Henderson and R.J. Speedy, Melting temperature of ice at positive and negative pressures, *J. Phys. Chem.* **91**, 3069 (1987).

61. D.R. Caldwell, The maximum density points of pure and saline water, *Deep-Sea Res.* **25**, 175 (1978).

62. S. J. Henderson and R. J. Speedy, Temperature of maximum density in water at negative pressure, *J. Phys. Chem.* **91**, 3062 (1987).

63. D.M. Murphy and T. Koop, Review of the vapour pressures of ice and supercooled water for atmospheric applications, *Q. J. R. Meteorol. Soc.* **131**, 1539 (2005).

64. A. Kostrowicka Wyczalkowska, Kh. S. Abdulkadirova, M. A. Anisimov, and J. V. Sengers, Thermodynamic properties of H_2O and D_2O in the critical region, *J. Chem. Phys.* **113**, 4985 (2000).

65. S. Sastry, P. G. Debenedetti, F. Sciortino, and H. E. Stanley, Singularity-free interpretation of the thermodynamics of supercooled water, *Phys. Rev. E* **53**, 6144 (1996).

66. L. P. N. Rebelo, P. G. Debenedetti, and S. Sastry, Singularity-free interpretation of the thermodynamics of supercooled water. II. Thermal and volumetric behavior, *J. Chem. Phys.* **109**, 626 (1998).

67. C. A. Angell, Insights into phases of liquid water from study of its unusual glass-forming properties, *Science* **319**, 582 (2008).

68. R. J. Speedy, Stability-limit conjecture. An interpretation of the properties of water, *J. Phys. Chem.* **86**, 982 (1982).
69. R. J. Speedy, Limiting forms of the thermodynamic divergences at the conjectured stability limits in superheated and supercooled water, *J. Phys. Chem.* **86**, 3002 (1982).
70. V. Molinero and E. B. Moore, Water modeled as an intermediate element between carbon and silicon, *J. Phys. Chem. B* **113**, 4008 (2009).
71. F. H. Stillinger and A. Rahman, Improved simulation of liquid water by molecular dynamics, *J. Chem. Phys.* **60**, 1545 (1974).